

Optical spectroscopy of BL Lac objects: TeV candidates

Simona Paiano^{1,2,3*}, Renato Falomo⁴, Aldo Treves^{3,5}, Riccardo Scarpa^{6,7}

¹INAF - Osservatorio Astronomico di Roma, via Frascati 33, I-00040, Monteporzio Catone, Italy

²INAF - IASF Milano, via Corti 12, I-20133, Milano, Italy

³Università dell'Insubria, via Valleggio, 22100, Como, Italy

⁴INAF - Osservatorio Astronomico di Padova, vicolo dell'Osservatorio 5, I-35122, Padova, Italy

⁵INAF - Osservatorio Astronomico di Brera, via Bianchi 46, I-23807, Merate (Lecco), Italy

⁶Instituto de Astrofísica de Canarias, C/O Via Lactea, s/n E38205 - La Laguna (Tenerife) - SPAIN

⁷Universidad de La Laguna, Dpto. Astrofísica, s/n E-38206 La Laguna (Tenerife) - SPAIN

Received: 25 June 2020; Accepted:

ABSTRACT

We investigate the spectroscopic optical properties of gamma-ray sources detected with high significance above 50 GeV in the Third Catalog of Hard Fermi-LAT Sources (3FHL) and that are good candidates as TeV emitters. We focus on the 91 sources that are labelled by the *Fermi* team as BL Lac objects (BLL) or Blazar candidates of uncertain type (BCU), that are in the Northern hemisphere, and are with unknown or uncertain redshift. We report here on GTC spectra (in the spectral range 4100 – 7750 Å) of 13 BCU and 42 BLL. We are able to classify the observed targets as BLL and each source is briefly discussed. The spectra allowed us to determine the redshift of 25 objects on the basis of emission and/or absorption lines, finding $0.05 < z < 0.91$. Most of the emission lines detected are due to forbidden transition of [O III] and [N II]. The observed line luminosity is found lower than that of QSOs at similar continuum and could be reconciled with the line-continuum luminosity relationship of QSOs if a significant beaming factor is assumed. Moreover for 5 sources we found intervening absorption lines that allows to set a spectroscopic lower limit of the redshift. For the remaining 25 sources, for which the spectra are lineless, a lower limit to z is given, assuming that the host galaxies are giant ellipticals.

Key words: galaxies: active and redshifts — BL Lacertae objects: general — gamma-rays: galaxies

1 INTRODUCTION

BL Lac objects (BLL) are active galactic nuclei, whose emission is dominated by non-thermal radiation from a relativistically beamed jet aligned with the line of sight. The emission, of synchrotron-inverse Compton origin, extends over the whole electromagnetic spectrum, from radio to gamma-ray. Distinctive characteristics of the class are the large and rapid flux variability, high polarization, and the absence or weakness of spectral lines, washed out by the emission from the jet, that in most cases makes very arduous the determination of their distance.

Data-sets of BLL have been produced through a number of dedicated surveys in all spectral bands, originally in the radio (Stickel, et al. 1991; Giommi, et al. 2002; Marchã & Caccianiga 2013), and X-rays (Stoeckle, et al. 1990; Perlmutter, et al. 1996, 1998; Laurent-Muehleisen, et al. 1998, 1999; Voges, et al. 1999; Cusumano, et al. 2010), then in the op-

tical and infrared (e.g. Scarpa, et al. 2000a; Scarpa, et al. 2000b; Urry, et al. 2000; Falomo, et al. 2000; Plotkin, et al. 2010; D'Abrusco, et al. 2014, 2019), and more recently also in the gamma-ray band (Abdollahi, et al. 2020, and references therein). The latter surveys indeed showed that BLL represent the dominant extragalactic population of gamma sources (The Fermi-LAT collaboration 2019). Thanks to its systematic monitoring of the whole sky, and the long duration of the mission, the *Fermi* catalogues of γ -ray sources have become a privileged means for discovering new BLL. The procedure of identification of the counterpart of the gamma-ray emitter generally goes through the search of X-ray and radio sources in the gamma-ray error box (e.g. Stephen, et al. 2010; Takeuchi, et al. 2013; Landi, et al. 2015; Paiano, et al. 2017). The BLL nature of the target can be guessed because of the broad spectral energy distribution (SED), which in BLL is well characterized by two broad humps, one due to synchrotron radiation (IR-optical), and one to inverse Compton (X-ray- Gamma rays). (see e.g. Maraschi, et al. 1992; Ghisellini & Tavecchio 2009;

* E-mail: simona.paiano@inaf.it

(Ghisellini, et al. 2017; Madejski & Sikora 2016). However, the secure classification derives generally from optical spectroscopy. The identification of weak spectral lines is the basic tool for obtaining first of all a firm classification and the distance of the source, but also for constraining some physical parameters of the emission region. If no intrinsic lines are observed, there are indirect procedures based on some hypothesis on the nature of the host galaxy, which can effectively produce lower limit to the redshift of the source (e.g. Sbarufatti, et al. 2006a; Sbarufatti, et al. 2006b; Meisner & Romani 2010; Falomo, Pian & Treves 2014, see also Section 4 of this paper). In some cases the optical spectra can exhibit absorption lines due to intervening medium, from which a spectroscopic lower limit to z can be derived.

The knowledge of the distance is a basic ingredient for modeling the BLLs, for constructing the luminosity function of this class of blazars, to assess the cosmic evolution, and to evaluate the contribution of the BLL population to the gamma-ray cosmic background. Because the overall spectrum may extend to the TeV domain, BLL of known redshift are unique probes of the extragalactic background light (EBL), since at $z \geq 1$ the absorption effects due to pair production become important (Franceschini, et al. 2017). Some BLL are also supposedly ultrahigh energy (PeV) neutrino emitters (Ahlers & Halzen 2015; Padovani, et al. 2016; Righi, et al. 2019), and again the distance knowledge is a crucial information for modeling the neutrino production, and the cosmic neutrino background radiation.

All these arguments explain the major effort for optical spectroscopic studies of BLL candidates. Because of the above mentioned weakness of the lines, it is compulsory to secure spectra with high and adequate signal-to-noise (S/N) ratios, in order to be able to measure these features of very low equivalent widths (EW). This requires the use of telescopes of the 8-10 m class.

For twenty years, we have embarked on a systematic study of BLL, lately focusing on *Fermi* detections, using the ESO 8 m Very Large Telescope (VLT) and, more recently, the 10 m Gran Telescopio Canarias (GTC). Optical spectra of ~ 250 BLL have been produced, adopting various selection criteria of the sources (Sbarufatti, et al. 2005a, 2006a, 2008, 2009; Landoni, et al. 2012, 2013, 2014, 2015; Paiano, et al. 2016; Falomo, et al. 2017; Paiano et al. 2017a,b,c, 2018; Landoni, et al. 2018; Paiano et al. 2019).

Here we present optical spectroscopy of 55 objects, which exhibit a hard gamma-ray spectrum in the 3FHL catalogue (Ajello, et al. 2017). From these observations, we are able to characterize the optical spectral properties and we determine the redshift in many objects.

In a coordinated paper (Paiano et al, in preparation), we will point out candidates for detection in the TeV range on the basis of the extrapolation to the very high energy ($> \sim 100$ GeV) of the *Fermi* spectra accounting for absorption by the EBL. It is expected that $\sim 20\%$ of the sources with known redshift considered in this work could be detected with the current Cherenkov telescopes, like MAGIC, and 85% with the future Cherenkov Telescope Array (CTA).

2 THE SAMPLE

The objects in our sample were extracted from the 3FHL catalog, which contains 1556 objects detected above > 10 GeV over 7 years of *Fermi* operations. We concentrate on 246 *TeV candidates*¹, which are sources revealed with significance > 3 at energy > 50 GeV. They exhibit a hard spectrum, with photon index $\Gamma \lesssim 2.5$ and integrated flux $F(>10 \text{ GeV}) \gtrsim 10^{-11} \text{ ph cm}^{-2} \text{ s}^{-1}$. Of these, 224 sources are classified by the *Fermi* team as BLL and blazar candidates of uncertain type (BCU): 180 and 44 sources respectively. Extensive search in the literature show that 153 of these objects lack a measurement of the redshift or the available value is uncertain. Of these, there are 21 BCU and 70 BLL at $\delta > 20$ and thus well-observable in the Northern hemisphere.

Here we report on extensive optical spectroscopy obtained at the GTC for 42 BLL and 13 BCU (see Table 1 for the properties of our sample).

3 OBSERVATIONS AND DATA REDUCTION

Optical spectra were collected using the spectrograph OSIRIS (Cepa, et al. 2003) of the 10.4 m GTC at the Roque de Los Muchachos (La Palma). We used the grism R1000B covering the spectral range 4100 - 7750 Å, and a slit width = 1.2".

Data reduction was performed using the IRAF software (Tody 1986, 1993) and standard procedures for long slit spectroscopy, following the same scheme given in Paiano et al. (2017a,b, 2019). For each source at least three spectra were obtained and combined together to obtain the final spectrum. Cosmic rays were removed using the L.A.Cosmic algorithm (van Dokkum 2001). The accuracy of the wavelength calibration is ~ 0.1 Å over the whole observed spectral range. The relative flux calibration was performed from the observation of a number of spectro-photometric standard stars secured during each night of the program. Since most of the spectra were obtained during non-photometric nights, we set the absolute calibration from the comparison of the magnitude of the targets, as from the acquisition image in the g band, and that of secondary photometric objects in the field as derived from PanSTARRS or SDSS images. Finally all spectra were dereddened applying the extinction law by Cardelli, Clayton & Mathis (1989) and assuming the value of Galactic extinction $E(B-V)$ derived from the NASA/IPAC Infrared Science Archive ² (Schlafly & Finkbeiner 2011). In Fig. 1, we display all our absolute-calibrated and dereddened spectra (*upper panel*) with the normalized form (*bottom panel*) obtained through the fit of the continuum with a cubic spline. The spectra are also available in our online database ZBLAC³.

4 METHODS AND RESULTS

For each spectrum the S/N was measured, and the minimum detectable EW was evaluated following the procedure described in detail in Paiano et al. (2017a).

The optical spectrum is assumed to be the superposition of a non thermal component described by a power law (PL) and the starlight component of the host galaxy. The latter is in almost all cases a giant elliptical galaxy of $M(R) \sim -22.9$ (Sbarufatti, et al. 2005b). We performed a spectral decomposition using these two components for all our targets (see some examples in Fig. 2)

¹ flagged as "C" in the 3FHL catalog

² <http://irsa.ipac.caltech.edu/applications/DUST/>

³ <http://web.oapd.inaf.it/zblac/>

and for details for the individual sources are reported in the corresponding notes. The visibility of the absorption features due to the host galaxy at a given wavelength, depends on the ratio of the two components (N/H, nucleus-to-host ratio) and on the minimum detectable EW (Sbarufatti, et al. 2006a). Under this assumption, it is possible to set a lower limit to the redshift, when no absorption lines of the host galaxy are detected. We followed the procedure described in the Appendix A of Paiano et al. (2017a) to evaluate this redshift lower limit.

Our optical spectroscopy shows that all 55 observed targets are BLL, including the 13 targets previously classified as BCU. No objects like flat spectrum radio-quasar or narrow line Seyfert I were found. In Tab 2 we report for each target whether the spectrum exhibits emission lines (labelled as E), galactic lines (G), intervening lines (I) or if it is lineless (L). For each source we give the redshift, the spectroscopic redshift lower limit in case of intervening line detection or a lower limit, estimated following the minimum EW method (described above), when the spectrum is featureless. In Table 3, we give the measurement of the all detected lines and in Fig. 3 we display some close-ups of the normalized spectra around interesting detected features. In 12 objects we detected emission lines and in 20 we found intrinsic absorption lines. This allows us the determination of 26 new redshifts, ranging from $z = 0.05$ to $z = 0.91$. The mean value is ~ 0.28 . In 5 sources intervening lines are detected, in most case due to Mg II, which enable to set a robust spectroscopic lower limit to the redshift. These intervening lines are originated at redshift in the range between 0.1 and 1.1. The intervening lines are an efficient tool for finding the most distant sources. For the reminder 24 sources, we provide the redshift lower limits based on lack of detection of spectral features. These limits range from $z > 0.1$ to $z > 0.6$.

5 NOTES ON INDIVIDUAL SOURCES

3FHL J0009.4+5030: The spectrum appears featureless and no emission/absorption lines are detected. On the basis of the minimum EW (~ 0.20 Å) and on the lack of detection of features from the host galaxy, we can set a redshift lower limit of $z > 0.6$.

3FHL J0015.7+5551: The observed optical counterpart ($g = 18.7$) of this gamma-ray source is at (RA,DEC)=(00:15:40, +55:51:45) and spatially coincident there is one X-ray source (J001540+555144), detected by *Swift*, and one radio source (NVSS J001540+555144). The de-reddened ($E(B-V) = 0.37$) spectrum of the source is characterized by stellar absorption features of the host galaxy (Ca II 3934,3968, G-band 4305, Ca+Fe 5269) at $z = 0.2168$, superposed to a non thermal power law continuum ($F_\lambda \propto \lambda^\alpha$, $\alpha = -1.2$). From the spectral decomposition of the two components, we set a $N/H = 1.5$. This object was previously studied by Álvarez Crespo, et al. (2016), who due to low S/N of the spectrum failed to detect the absorption features. At $\sim 2.5''$ (West on the right), there is a faint companion ($g = 20.7$) that was placed in the slit during our observation and exhibits a stellar spectrum.

3FHL J0045.3+2127: Our optical spectrum (S/N ~ 90) is characterized by a power law emission ($\alpha = -1.3$). We detect a faint absorption doublet at ~ 5600 Å that we identify as Ca II 3934,3968 at $z = 0.4253$. It is worth to note that there is a galaxy close to our target at a projected distance of $\sim 10''$ (see Fig. 4) with redshift $z = 0.4265$ provided by SDSS survey. A previous spectrum provided by SDSS survey failed to detect any feature, while Shaw, et al. (2013) provided a lower limit compatible with our measurement.

3FHL J0045.7+1217: In our spectrum we find absorption lines due to Ca II 3934,3968, G-band 4305, Mg I 5175 and Ca+Fe 5269 attributed to the stellar population of the host

galaxy. In addition we also detect a faint (EW = 0.2 Å) emission line due to [O II] 3727 (see Fig. 3). The redshift is 0.2549. This is consistent with the lower limit proposed by Shaw, et al. (2013). From the spectral decomposition, we set a $N/H \sim 4.5$ and $\alpha = -1.0$ for the nuclear power law component.

3FHL J0131.1+6120: The dereddened spectrum ($E(B-V) = 0.79$) is featureless with a minimum detectable EW varying between 0.20 Å and 0.70 Å along the spectrum. We can set a lower limit of the redshift $z > 0.10$.

3FHL J0134.4+2638: We obtain an optical spectrum that is featureless. No emission or absorption lines are detected out to a minimum EW of 0.35 - 0.50 Å. This is consistent with the featureless spectrum of the SDSS survey. From the lack of detection of host galaxy features, we can set a redshift lower limit $z > 0.15$. An optical spectrum obtained by Marchesi, et al. (2018) exhibits a prominent emission line at ~ 4400 Å which is interpreted as Mg II 2800. We suspect that the reported line is a spurious artifact. In fact this feature is not reported in the SDSS spectrum and in Shaw, et al. (2013).

3FHL J0137.9+5815: Our spectrum (S/N ~ 145) is dominated by non-thermal continuum. We detect very weak absorption features from the host galaxy (Ca II 3934,3968, Mg I 5175 and Ca+Fe 5269), yielding a $z = 0.2745$, and from the spectral decomposition we obtain $N/H \sim 3$. No previous spectrum is available in literature.

3FGL J0141.4-0929: The only feature in our spectrum is an absorption doublet at ~ 4200 Å, which is due to intervening Mg II 2800, yielding a spectroscopic lower limit of the redshift of $z \geq 0.501$. This feature is also present in the spectra reported in Stickel, et al. (1993) and Stocke, et al. (1997). Note that we do not confirm the emission of Mg II 2800 and [O II] 3727 at $z = 0.737$ proposed by Stocke, et al. (1997).

3FHL J0148.2+5201: In our spectrum, the Ca II 3934,3968 doublet is apparent at ~ 5670 Å and, together with the G-band 4305 absorption line at 6183 Å, yield $z = 0.437$. The decomposition of the spectrum provides a $N/H \sim 5$, and $\alpha = 1.3$ for the nuclear power law component. The spectrum published by Álvarez Crespo, et al. (2016), with a poorer S/N, is featureless.

3FHL J0241.3+6543: We detect two emission lines at ~ 7370 Å which can be interpreted as H_α 6563 and [N II] 6584 at $z = 0.1211$ (see the close-up in Fig. 3). At the same redshift, there is a further emission doublet that we attribute to [S II] 6716,6731, and an absorption line due to Na I 5892. We note that Marchesi, et al. (2018), on the basis of an absorption doublet at ~ 4600 Å, identified as Mg II, suggest a redshift lower limit $z \geq 0.645$. This conflicts with our redshift determination.

3FHL J0250.5+1712: We obtain a spectrum with S/N ~ 100 which exhibits clear absorption lines attributed to the host galaxy (Ca II 3934,3968, H_δ 4861, G-band 4305, Mg I 5175, H_β 4861 and Na I 5892). This yields a redshift of $z = 0.2435$, confirming the proposal of Archambault, et al. (2016). For the emission lines, the upper limit of EW is ~ 0.45 Å. The present of the host galaxy is well detected in the decomposition reported in Fig. 2, where a $N/H = 2$ is estimated.

3FHL J0322.0+2336: Our optical spectrum, with S/N >160 , is largely superior to one reported by Laurent-Muehleisen, et al. (1998), but still no significant features are present. The upper limit for the emission/absorption lines is EW = 0.10 - 0.25 Å, corresponding to a lower limit of the redshift of $z > 0.25$.

3FHL J0423.8+4149: We detect a single emission line at 6997.6 Å of equivalent width EW = 1.9 Å. The most plausible identification of this line is [O III] 5007 that yields a tentative redshift of $z = 0.3977$. The other component of [O III] 4959 doublet is washed out by the telluric band at 6870 Å. This target was

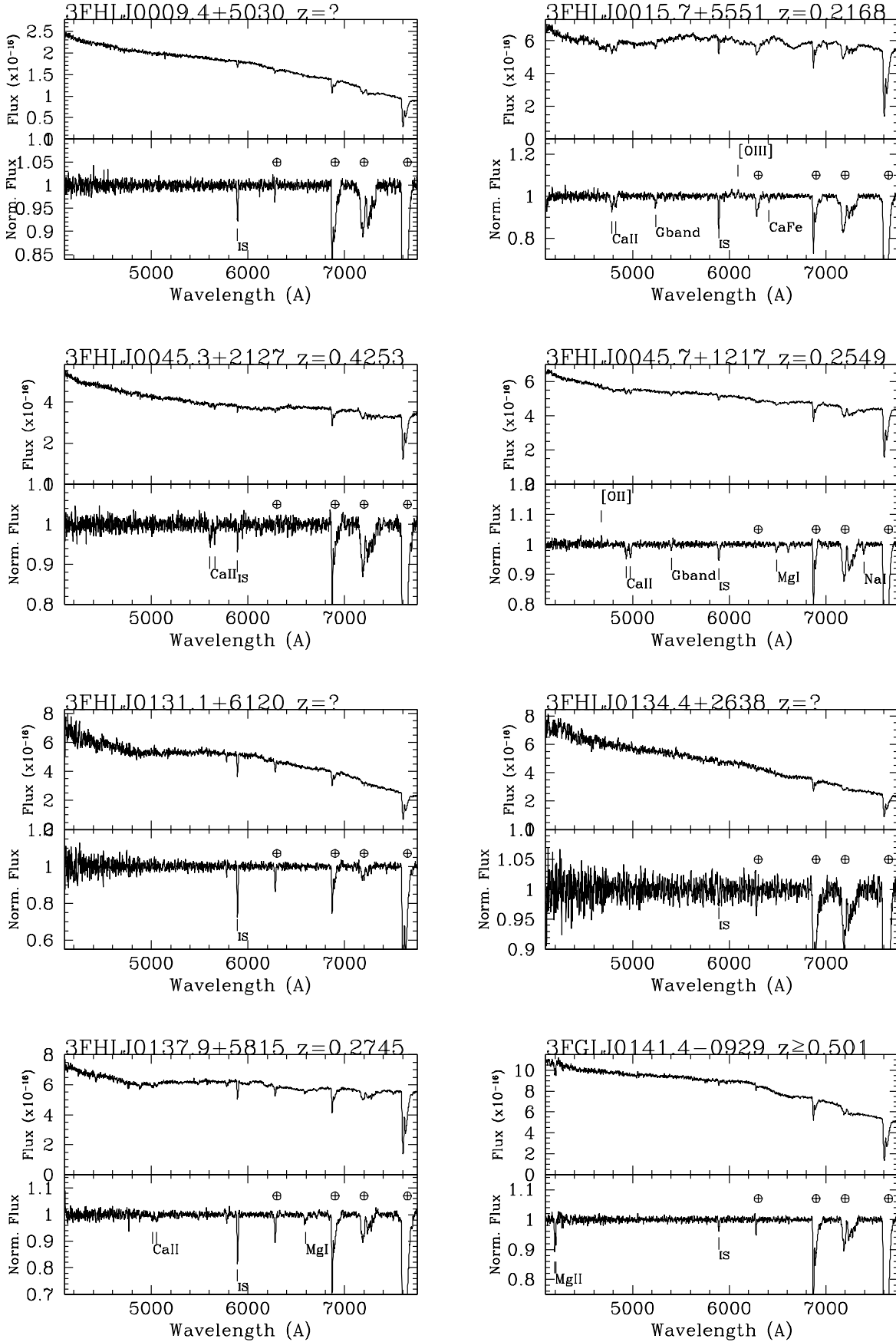


Figure 1. Spectra of the UGSs obtained at GTC. *Top panel:* Flux calibrated and dereddened spectra. *Bottom panel:* Normalized spectra. The main telluric bands are indicated by \oplus , the absorption features from interstellar medium of our galaxies are labelled as IS (Inter-Stellar)

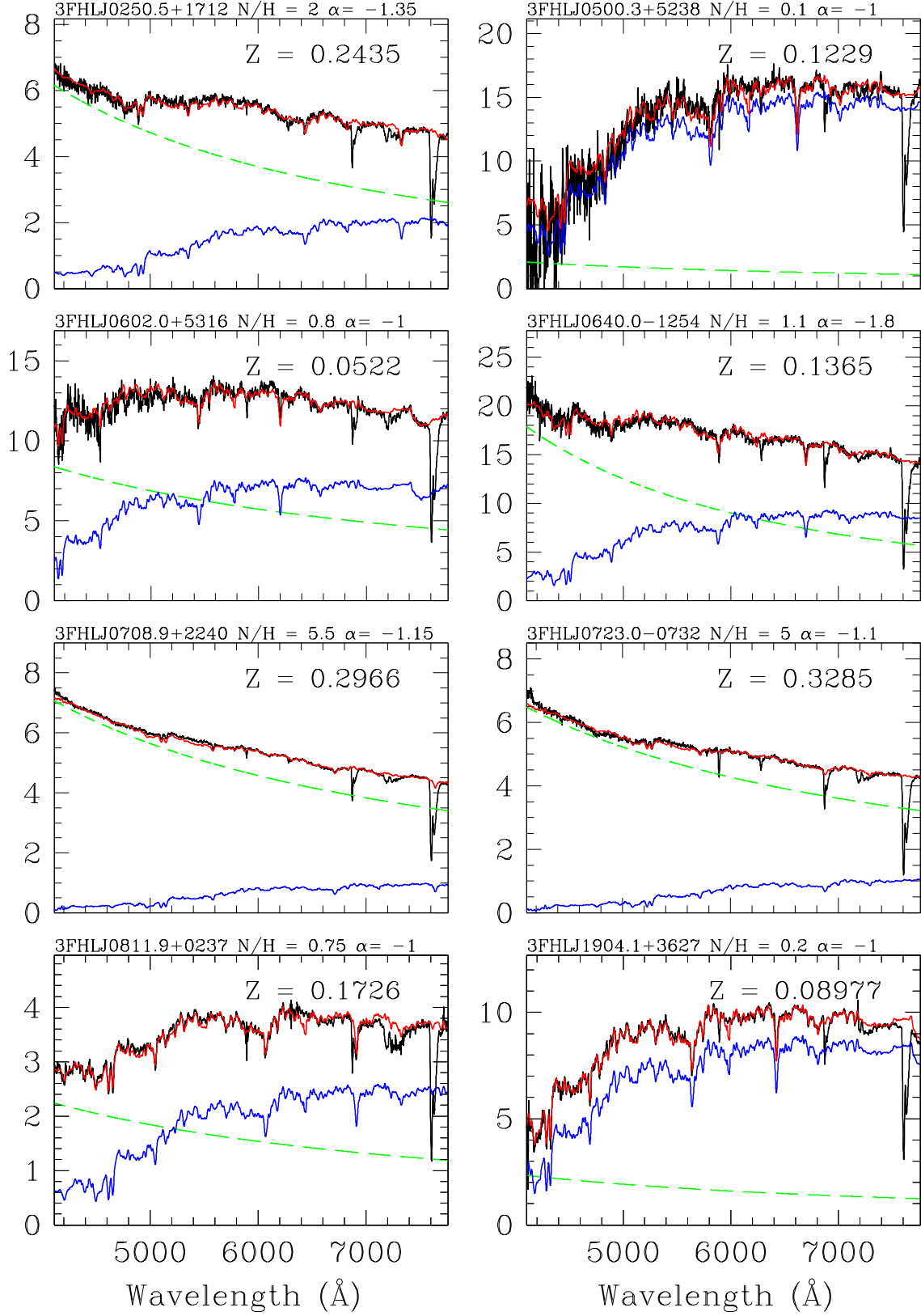


Figure 2. Spectral decomposition of the observed optical spectrum (black line) of selected targets into a power law (green dashed line) and a template of elliptical for the host galaxy (blue line). The fit is given by the red solid line (see text for details). On each panel the nucleus to host ratio is given together with the spectral index of the power law component.

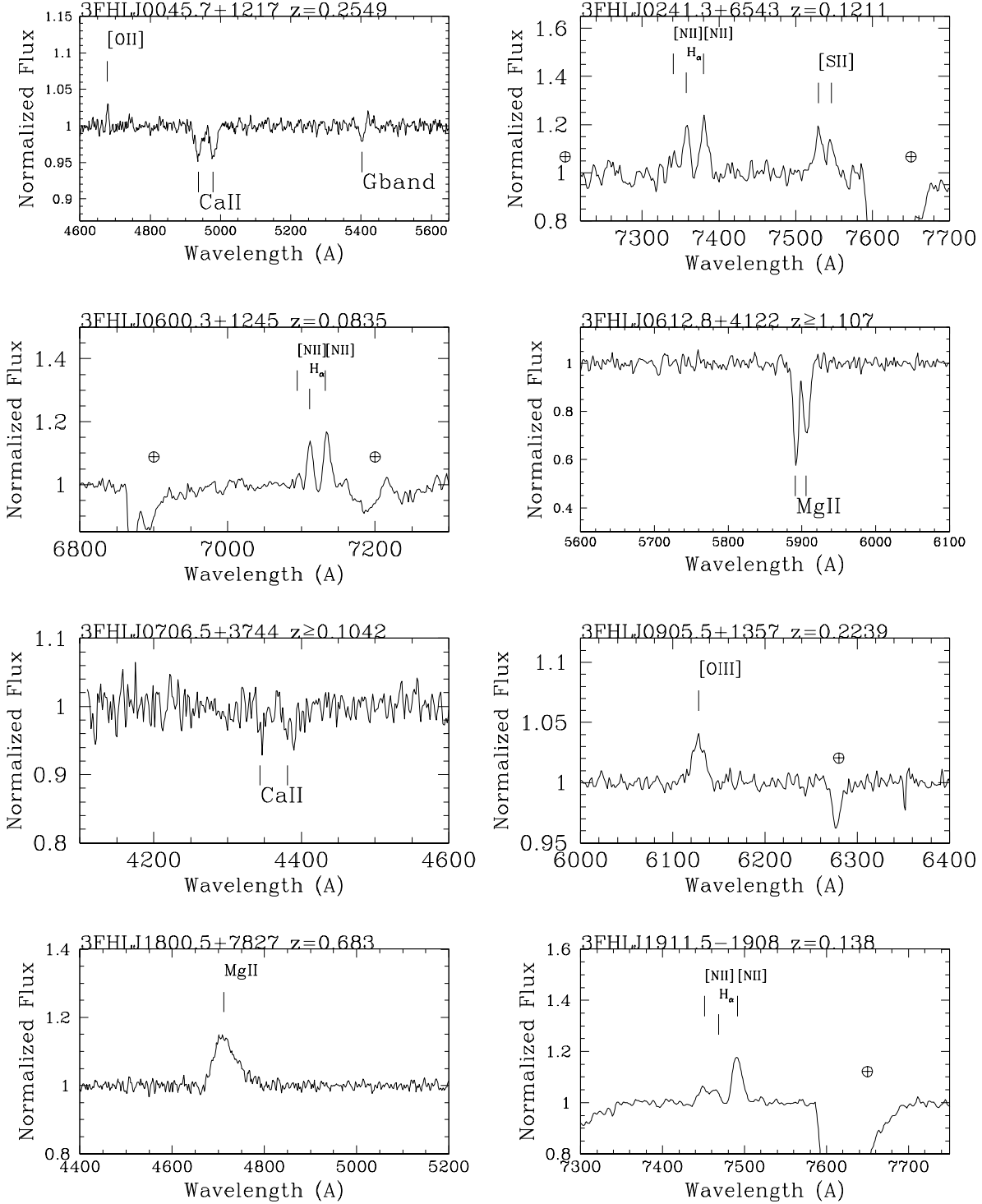


Figure 3. Some examples of close-up of the normalized spectra, obtained at GTC of the 3FHL TeV candidate objects, around the detected spectral lines. Main telluric bands are indicated as \oplus , spectral lines are marked by line identification.

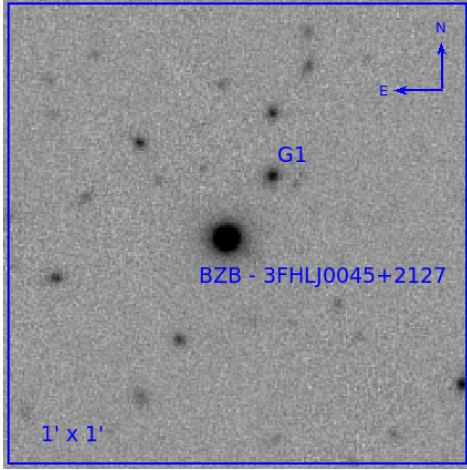


Figure 4. PANSTARR *i*-band image of the BLJ 3FHL J0045+2127. There is one close companion at $\sim 10''$ from the target (that is at the center). Field shown is $1' \times 1'$, North up and East left.

proposed as neutrino source by Righi, et al. (2019) and Paiano et al. (2019).

3FHL J0433.1+3227: Even though our optical spectrum ($S/N \sim 100$) is of higher quality than that presented by Álvarez Crespo, et al. (2016) ($S/N \sim 5$), we still do not find significant features and from the minimum detectable $EW \sim 0.3 \text{ \AA}$, we can set a redshift lower limit $z > 0.45$.

3FHL J0433.6+2905: The spectrum is severely reddened with $E(B-V) = 0.66$. There is a possible broad emission feature centered at $\sim 5340 \text{ \AA}$ in a region of the spectrum where the $S/N \sim 15$. A similar feature maybe is present in the spectrum reported in Shaw, et al. (2013), but not identified by the authors. Supposing that this feature is due Mg II 2800, the redshift would be ~ 0.91 .

3FHL J0434.7+0921: In our spectrum no spectral feature is apparent. We set a lower limit of $z > 0.1$ from the lack of absorption lines from the host galaxy.

3FHL J0500.3+5238: The target is highly reddened with $E(B-V) = 0.75$. Several photospheric absorption lines are apparent (G-band 4305, H_β 4861, Mg I 5175, Na I 5892 and H_α 6564), yielding $z = 0.1229$. At the same redshift there is a narrow emission line attributed to [N II] 6584 with $EW \sim 1.3 \text{ \AA}$. The spectral decomposition in the power law ($\alpha \sim -1.0$), due to the nucleus, and in the host galaxy template is reported in Fig. 2 and we find a $N/H = 0.1$.

3FHL J0506.0+6113: The optical spectrum ($S/N \sim 70$) is highly reddened with $E(B-V) = 0.55$. We find a hint of Ca II 3934,3968 doublet at 6042,6096 \AA that would correspond to $z \sim 0.54$.

3FHL J0515.8+1528: No significant feature is apparent in our spectrum ($S/N \sim 130$). From the null detection of absorption lines of the host galaxy, we can set a lower limit of $z > 0.2$.

3FHL J0540.5+5823: There are no convincing emission/absorption features in our spectrum ($S/N \sim 60$). A lower limit of $z > 0.10$ can be set from the lack of detected absorption lines of the host galaxy. This source is inserted in the Padovani, et al. (2016) list of hard gamma-ray sources found around the position of IceCube events.

3FHL J0600.3+1245: This gamma-ray object, associated to the radio source NVSS J060015+124344, is classified as BCU in the *Fermi* catalogs. It is spatially coincident with the X-ray source 1RXS J060014.8+124341 and with the optical counterpart

at (RA,DEC) = (06:00:15, 12:43:43). Our optical spectrum exhibits several absorption lines (G-band 4305, H_β 4861, Mg I 5175, Na I 5892 and H_α 6563) attributed to the old stellar population of the host galaxy, that allow us to measure $z = 0.0835$. At the same redshift, we also detect, at $\sim 7133 \text{ \AA}$, two narrow emission lines ($EW = 1.2 \text{ \AA}$ and $EW = 1.8 \text{ \AA}$) due to H_α 6563 and [N II] 6584 (see the close-up in Fig. 3).

3FHL J0601.0+3837: The source was proposed as a BLL by Paggi, et al. (2014) who show a featureless spectrum of the X-ray counterpart. The source is faint ($g = 20.5$) and severely extinguished ($E(B-V) = 0.46$), and we obtained a spectrum with a $S/N \sim 40$. This is basically featureless, apart for a possible doublet (at $\sim 6560 \text{ \AA}$) that, if attributed to Ca II doublet of the host galaxy, corresponds to a redshift $z = 0.662$.

3FHL J0602.0+5316: The gamma-ray source is associated to the bright radio galaxy GB6J601+5315 and it is inside the error box of a neutrino event detected by IceCube (Padovani, et al. 2016). No previous optical spectrum is found in literature. Our spectrum of the source ($g = 17.0$) shows the absorption lines (Ca II, G-band, etc...) of the galaxy stellar population at $z = 0.0522$. The decomposition of the optical spectrum (see Fig. 2) in an elliptical template and power-law ($\alpha \sim -1.0$) emission indicates the presence of a **non-thermal** component contributing for $\sim 45\%$.

3FHL J0607.4+4739: An optical spectrum, obtained by Shaw, et al. (2013), does not show any significant features. From our lineless spectrum ($S/N = 100$), on the basis of the lack of detectable galaxy absorption lines, we can set a redshift lower limit $z > 0.10$.

3FHL J0612.8+4122: Our spectrum is dominated by a power law continuum without significant intrinsic emission/absorption lines. However, we clearly detect intervening absorption systems of Mg II 2800, Fe II 2382, and Fe II 2586,2600 at $z = 1.107$. The Mg II absorption line doublet is also apparent in Shaw, et al. (2013).

3FHL J0620.6+2645: This gamma-ray source ($g = 18.5$) is classified as BCU in the *Fermi* catalogs. No previous optical spectrum is available. In our spectrum, many absorption lines from the host galaxy are clearly detected, yielding $z = 0.1329$. The decomposition of the spectrum, in a elliptical galaxy and a power law ($\alpha = -1.5$) emission, allows us to set $N/H \sim 0.5$.

3FHL J0640.0-1254: No previous redshift is reported in literature. Our spectrum exhibits absorption lines (Ca II, G-band, Mg I, Na I) of the host galaxy diluted by the non thermal emission from the nucleus, allowing to measure $z = 0.1365$. The spectral decomposition in the elliptical galaxy and nucleus power law component provides an $N/H \sim 1$ (see Fig. 2). In addition to the absorption feature, we also detect a narrow emission line at 7482 \AA ($EW = 0.6 \text{ \AA}$) corresponding to [N II] 6584. We note that the object visible at $6.5''$ from the target is a star and it is derived by the GTC spectrum obtained during the same observation of our target.

3FHL J0702.6-1950: No optical spectra are found in literature. We obtain the spectrum orientating the slit to intersect the target ($g = 19.1$) and the close object at $\sim 5''$, which is a star (the classification is provided by GTC spectroscopy). The moderate $S/N \sim 50$ spectrum of the γ -ray target is dominated by a featureless continuum characterized by a typical power law shape with spectral index $\alpha = -1.4$. Based on the lack of spectral features from the host galaxy, we set a lower limit of $z > 0.10$.

3FHL J0706.5+3744: We detect a faint absorption doublet at $\sim 4350 \text{ \AA}$ ($EW \sim 0.6 \text{ \AA}$) that is attributed to Ca II 3934,3968 (see Fig. 3) yielding the redshift $z = 0.1042$. If these lines were ascribed to the starlight of the host elliptical galaxy, we would expect to observe the trace of the host galaxy in the continuum, which is not present. Moreover these detected lines are narrower,

compared to the typical Ca II line width from elliptical galaxies, rather indicating an interstellar absorption origin. Indeed at $\sim 12''$ from the target, there is another galaxy for which we obtained an optical spectrum: we found several emission lines due to H β 4861, [OIII] 4959,5007 and H α 6563 at $z = 0.1042$, the same value of the BLL. We suppose that the halo gas of this close galaxy (located at the projected distance ~ 23 kpc at that redshift) can be responsible of the absorption doublet found in the spectrum of γ -ray source. Therefore, for 3FHL J0706.5+3744, we set the spectroscopic lower limit of the redshift $z \geq 0.1042$.

3FHL J0708.9+2240: This object is a BCU γ -ray emitter associated to the radio source GB6J0708+2241. The optical counterpart ($g = 17.4$) is at (RA,DEC)=(07:08:58.3, 22:41:36.0). Massaro, et al. (2015) report an optical spectrum without evident features. We detect absorption lines (Ca II, G-band, and Mg I) due to the old stellar population of the host galaxy, allowing us to locate the source at $z = 0.2966$. The spectral decomposition, reported in Fig. 2), indicates the presence of a no-thermal power law component ($\alpha = -1.15$) and a N/H = 5.5.

3FHL J0709.1-1525: In the *Fermi* catalog, this BCU γ -ray source is associated to the radio source PKS 0706-15. From the analysis of *Swift*/XRT data, inside the Fermi error box we detect the X-ray source J070912-152703, spatially coincident with the radio counterpart and the optical counterpart ($g = 18.9$) at (RA,DEC)=(07:09:12.3,-15:27:00.0). This confirms the association with PKS 0706-15. No previous spectrum is reported in literature. Our spectrum, highly reddened ($E(B-V) = 0.55$), exhibits the shape of an elliptical galaxy with evident absorption lines (Ca II, G-band, H β , Ca+Fe, Na I, and H α) at redshift $z = 0.1420$. In addition we detect an emission line (EW = 1.0 Å) at 7518 Å which is attributed to [N II] 6584 Å.

3FHL J0723.0-0732: The blazar classification of this γ -ray emitter is proposed by Martí, et al. (2004) who report a featureless optical spectrum. In our spectrum (S/N ~ 170), we detect the absorption doublet attributed to Ca II 3934,3968 and a faint feature due to G-band. This yields a redshift of $z = 0.3285$. The decomposition of the spectrum (see Fig. 2) in an elliptical template and power-law emission indicates the presence of no-thermal component and allows us to set N/H ~ 5 .

3FHL J0811.9+0237: There are not previous spectra available for this object. Our spectrum clearly exhibits absorption lines (Ca II, G-band, H β , Mg I, Ca+Fe, and Na I) due to the host elliptical galaxy at $z = 0.1726$. In addition a faint emission line attributed to [N II] 6584 is detected at the same redshift. The decomposition of the spectrum in an elliptical galaxy and power-law ($\alpha = -1$) emission reveals the presence of no-thermal component and the N/H ~ 0.75 (see Fig. 2). We note that 3FHL J0811.9+0237 could belong to a small group of galaxies. There are two neighbour galaxies at $\sim 9''$ (on East) and $\sim 22''$ (North-West) at redshift similar to our target (see Fig. 5): from our GTC spectroscopy of G1 and from the SDSS spectrum available for G2, we find that these companions are elliptical galaxies at $z = 0.1697$ of projected velocity of ~ 900 km s $^{-1}$ relative to our target.

3FHL J0816.4-1311: Despite the high quality optical spectrum (S/N ~ 300), no emission/absorption lines are found. On the basis of the minimum detectable EW (~ 0.10 Å) and the lack of feature detection from the host galaxy, we can set a redshift lower limit of $z > 0.40$. There are previous spectra reported in literature by Shaw, et al. (2013), who show a featureless spectrum, and by Pita, et al. (2014) that found intervening absorption systems attributed to Mg II 2800 (at $z = 0.1902$, $z = 0.2336$, and $z = 0.2882$) in a spectral range not covered by our spectrum.

3FHL J0905.5+1357: We observed this source at two different epochs separated by an interval of about one year (see Table 1). It is noticeable that the source magnitude obtained from the acquisition images varied by \sim one mag. In Fig. 1 we report

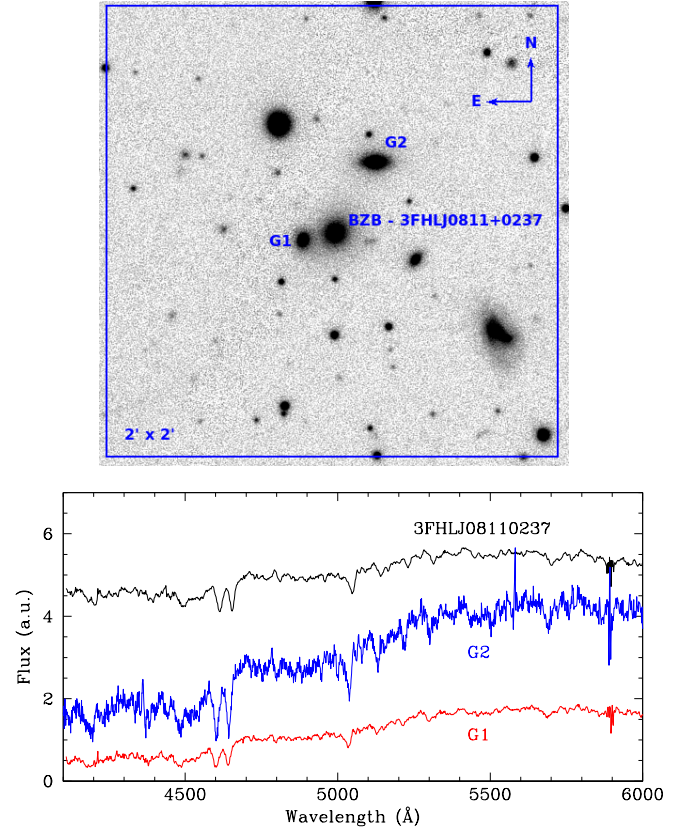


Figure 5. Upper panel: The PANSTARR *i*-band image (North up and East left) of the BLL 3FHL J0811.9+0237 (in the center). There are two close companions of the BLL: G1 at $\sim 9''$ and G2 at $\sim 22''$. Bottom panel: Comparison of the BLL spectrum with the spectra of the two companions (see details in the text).

the average spectrum of the two epochs. The shape is the typical BLL continuum and the only intrinsic feature detected is an emission line (average EW ~ 0.7 Å) at 6133 Å (see the close-up around this line in Fig. 3) which, if attributed to [OIII] 5007, yields a redshift of 0.2239. The line luminosity is $\sim 8 \times 10^{40}$ erg/s during the two states, while the continuous varies of a factor of ~ 3 . This source is quoted in Padovani, et al. (2016) as spatially coincident with the error box of a neutrino IceCube event and there are two previous spectra by Shaw, et al. (2013) and the SDSS. Both spectra appear featureless and correspond to a high state of the source ($F(6100\text{Å}) \sim 1 \times 10^{-16}$ erg cm $^{-2}$ s $^{-1}$) that probably has hampered the detection of the line, which appeared clearly in our observations when the source was in a lower flux state.

3FHL J0910.5+3329: Our optical spectrum with S/N ~ 200 appears featureless, in agreement with the previous spectra available in literature (Bauer, et al. 2000; Shaw, et al. 2013, and that provided by the SDSS survey). We can set a redshift lower limit $z > 0.15$ on the basis of the non-detection of features due to the host galaxy.

3FHL J0953.0-0840: The only spectrum available in literature is provided by Shaw, et al. (2013) that is featureless. In our good optical spectrum (S/N ~ 220), still no emission/absorption line is detected. The spectrum exhibits the power-law shape, typical for BLLs, with spectral index of $\alpha = -1.5$. By the minimum EW method, we can set the redshift lower limit $z > 0.15$.

3FHL J1037.6+5711: All previous spectra reported in literature (Laurent-Muehleisen, et al. 1998; Caccianiga, et al. 2002; Shaw, et al. 2013, and the SDSS survey) do not exhibit

emission/absorption lines. Our high quality (S/N~300) spectrum shows the typical BLL power-law shape and it still is featureless. The estimated minimum EW is ~ 0.15 Å and this yields a redshift lower limit $z > 0.25$.

3FHL J1055.6-0125: No redshift is reported in literature. The spectral shape of our spectrum is well described by a power law emission ($\alpha \sim -1.5$), typical of a BLL. No emission or absorption features are apparent at level of EW~0.40 Å and we can set a redshift lower limit of $z > 0.55$.

3FHL JJ1059.1-1134: The source was observed by [Landoni, et al. \(2013\)](#) and [Shaw, et al. \(2013\)](#) and they did not detect any features. Also our spectrum appears featureless. The minimum detectable EW spans between 0.30 Å and 1.15 Å along the spectrum, allowing us to set a redshift lower limit based on the lack of galaxy absorption lines of $z > 0.10$.

3FHL J1150.5+4154: There is an SDSS spectrum of the source and one in the collection of [Shaw, et al. \(2013\)](#). Neither absorption nor emission features are apparent. Also our high S/N~200 spectrum is featureless and from the minimum EW~0.25 Å, we can set a lower limit $z > 0.25$ from the lack of detection of features from the host galaxy.

3FHL J1233.7-0145: Optical spectra provided by [Shaw, et al. \(2013\)](#), [Kügler, et al. \(2014\)](#) and from the SDSS survey are featureless and no spectroscopic redshift is provided. Also in our spectrum no emission/absorption features are detected and, from a minimum detectable EW~0.45 - 0.95 Å, we can set a redshift lower limit of 0.10.

3FHL J1253.1+5300: In our high quality spectrum (S/N~250) of the target ($g = 16.6$), we detect a faint absorption doublet system (EW~0.3 Å) at ~ 4660 Å attributed to intervening Mg II Å cold gas, allowing us to set the spectroscopic redshift lower limit $z \geq 0.6638$. The same line system is found in the spectrum of the SDSS survey and reported by [Shaw, et al. \(2013\)](#).

3FHL J1418.4-0233: All optical spectra reported in literature ([Shaw, et al. 2013](#); [Kügler, et al. 2014](#), and that provided by SDSS survey) appear featureless and no redshift is measurable. Our S/N~200 optical spectrum of this bright target ($g = 16.4$) does not exhibit emission or absorption lines and the minimum detectable EW is ~ 0.15 -0.30 Å. We can set a redshift lower limit of $z > 0.12$.

3FHL J1445.0-0326: This object has been classified as BLL by [Bauer, et al. \(2000\)](#), but its redshift was not determined because of the absence of emission and absorption features. Featureless spectra are reported in [Sbarufatti, et al. \(2006a\)](#) and [Piranomonte, et al. \(2007\)](#). Also our spectrum (S/N = 200) does not show apparent spectral lines at level of EW~0.20 Å and we can set a redshift lower limit of $z > 0.45$.

3FHL J1447.9+3608: In our spectrum (SNR~250), there is a clear absorption doublet at 4865 Å, which is due to intervening Mg II 2800 system, yielding a spectroscopic lower limit of $z \geq 0.738$. The feature was noted by [Shaw, et al. \(2013\)](#) and appears also in the SDSS spectrum.

3FHL J1454.5+5124: The redshift $z = 1.0831$ reported in literature was proposed by the automatic procedure of the SDSS survey. However no convincing line identification is provided and also the spectrum shown by [Shaw, et al. \(2013\)](#) appears featureless. In our spectrum of very good quality, with S/N~320, no spectral features are found. We can set a redshift lower limit of $z > 0.40$ by the minimum EW~0.10 Å.

3FHL J1503.7-1541: The optical spectra reported in literature ([Bauer, et al. 2000](#); [Sbarufatti, et al. 2006a](#); [Shaw, et al. 2013](#)) are featureless. Also our spectrum does not present emission/absorption lines and we can set a redshift lower limit of $z > 0.10$.

3FHL J1549.9-0659: This gamma-ray emitter is associated

to the radio source NVSS J154952-065907 and proposed as blazar candidate in the *Fermi* catalog because no spectra are available in literature. Our spectrum establishes the BLL nature of the source and we find faint absorption lines due to Ca II 3934,3968 and G-band 4305, attributed to the stellar population of the host galaxy, at a $z = 0.418$.

3FHL J1748.6+7005: In literature, [Stickel, et al. \(1989\)](#) provided a tentative redshift of $z = 0.77$ based on identification of the very faint (EW = 0.4 Å) [O II] emission line at 6600 Å. This value was subsequently confirmed by [Lawrence, et al. \(1996\)](#) from the detection of additional lines due to C III] (EW = 0.4 Å) and [O III] (EW = 0.7 Å). Our high S/N (~300) spectrum of the bright target ($g = 16.6$) is featureless. Note that we cannot detect the emission lines claimed in the previous works because they are out of our spectral range.

3FHL J1800.5+7827: We clearly detect a significant (EW = 8.3 Å) emission line at 4712 Å (see the close-up in Fig. 3) that, if attributed to Mg II 2800, leads to a redshift $z = 0.683$. From the literature, a similar value is reported in [Hewitt, et al. \(1993\)](#) and in [Stickel, et al. \(1994\)](#) where neither spectrum nor line identification are shown.

3FHL J1841.3+2909: This 3FHL source is associated to the radio source MG3 J184126+2910 and proposed as BLL candidate ([Massaro, et al. 2013](#)). Our de-reddened ($E(B-V)=0.21$) optical spectrum is described as a power-law ($\alpha = -1.1$) and no evident lines are found. We set a redshift lower limit of $z > 0.1$. There is also another spectrum published by [Marchesi, et al. \(2018\)](#) that is again featureless.

3FHL J1904.1+3627: This target is a candidate blazar in the *Fermi* catalog and associated to the radio source MG2 J190411+3627. In [Marchesi, et al. \(2018\)](#) the optical spectrum seems featureless, mainly due to a poor S/N. Our spectrum (S/N~60) is modelled by an elliptical galaxy shape and shows several absorption lines due to the old stellar population of the host galaxy. The redshift of the target is $z = 0.08977$. From the spectral decomposition (see Fig. 2) we can determine that the AGN contributes to $\sim 15\%$ (N/H=0.2).

3FHL J1911.5-1908: This source is a BCU of the *Fermi* catalog associated to the radio source PMN J1911-1908. [Marchesi, et al. \(2018\)](#) report an optical spectrum of modest S/N that appears featureless. In our spectrum, several absorption lines are found due to the old stellar population (Ca II, G-band, Mg I, Ca+Fe and Na I), yielding a redshift $z = 0.138$. At the same redshift, we also detect narrow emission lines due to forbidden transitions attributed to [O II] 3727, [O III] 5007, [N II] 6548, H α 6563 partially blended, and [N II] 6584.

3FHL J1921.8-1607: Our good (S/N~125) optical spectrum does not exhibit emission or absorption lines. From the lack of detection of features of the host galaxy, with the minimum detectable EW~0.20-0.50 Å and magnitude $g = 17.6$, we can set a lower limit of the redshift $z > 0.12$. In literature, there is another spectrum in [Shaw, et al. \(2013\)](#) that is featureless.

6 SUMMARY AND CONCLUSIONS

From our optical spectroscopy, we can assess that all sources in the observed data set are BLL. We determined the redshift for 26 objects from absorption lines of their host galaxies and in some cases also from emission lines. For other 5 objects we found a spectroscopic lower limit from the detection of intervening absorptions. The remaining 24 sources have featureless optical spectra thus we estimate a redshift lower limit from the absence of absorption features of the host galaxy. Moreover for all the latter sources there are not intervening absorptions that suggests they are at relatively low redshift. Considering the absorptions from Mg II we expect that the number of Mg II absorbers per

redshift bin (dN/dz), with $EW > 0.3 \text{ \AA}$, is ~ 0.5 (Zhu & Ménard 2013). Since none are detected above 4100 \AA , one must have on average $\bar{z} < 0.6$. This is consistent with the median value of the detected redshifts ($\bar{z} \sim 0.3$).

BLL are characterized by the lack (or very weak) features in their optical spectra. Apart from the absorption lines from the host galaxies, that are always present if sufficient high quality spectrum is available (Landoni, et al. 2014), it is of interest to evaluate the properties of the possible emission lines compared with other active nuclei. Weak narrow emission lines are observed in a number of cases for BLL. These can arise either from a region of significant star formation or from nuclear emission in the narrow line region (Bressan, et al. 2006; Paiano et al. 2017a, 2018). The detection of weak broad emission lines is rarer (see e.g. Sbarufatti, et al. 2006b; Landoni, et al. 2012). It adds an important ingredient for the understanding of this class of active galactic nuclei (e.g. Giommi, et al. 2013), in particular in the connection with the FSRQ and the possibility of an evolutionary relation between these two classes (for example Giommi, et al. 2013; Ajello, et al. 2014).

In 4 objects we detected weak ($EW \sim 0.5\text{--}1.9 \text{ \AA}$) [O III] 5007 emission lines (see Table 3). This yields an average line luminosity $L \approx 8 \times 10^{40} \text{ erg/s}$. For the 13 objects of known redshift and for which [O III] would be observable in our spectra, on average we set an upper limit line luminosity of $3 \times 10^{40} \text{ erg/s}$. A similar limit was also derived for the 24 sources of unknown redshift, assuming that the [O III] emission line be inside the observed range. In addition to the [O III] emission line, we also detect [N II] 6584 emission feature in 7 targets (only in one of these cases also [O III] is present). The derived [N II] line luminosity is in the range $0.1\text{--}2 \times 10^{41} \text{ erg/s}$. Only for two sources we detected measurable H_α emission. These weak ($EW \sim 1.5 \text{ \AA}$) lines imply H_α luminosity of 2.5×10^{40} and $1.2 \times 10^{41} \text{ erg/s}$. At face value, the [O III] line luminosity is significantly lower than that found for the low redshift ($0.1 < z < 0.5$) QSOs (see e.g. Shen, et al. 2011) at comparable observed continuum luminosity (see Fig. 6-upper panel-a). On average the [O III] luminosity for our BLL sample is a factor ~ 50 lower than that found for the QSOs ($\sim 10^{42} \text{ erg/s}$) and a factor ~ 20 lower considering the [O III] luminosity distribution of the type II QSOs (see Zakamska, et al. 2003). This might indicate either that the lines are indeed fainter of that found in the QSOs at the same continuum level or that the continuum is significantly enhanced by the presence of relativistic beaming that is characteristic of this kind of sources (e.g. Urry & Padovani 1995). Actually, assuming a beaming factor of ~ 10 , both measured values and upper limits move to the region at the lowest line and continuum luminosities as it is displayed in Fig. 6-upper panel-b).

Another important result of our spectroscopy is that we do not find broad emission lines, except for 3FHL J1800.5+7827 for which we detect Mg II emission line of $EW = 8.3 \text{ \AA}$, $FWHM \sim 3500 \text{ km/s}$ and $L_{MgII} = 2.2 \times 10^{43} \text{ erg/s}$. This is at the limit of the distribution of the QSOs at similar redshift and luminosity of the continuum (see Fig. 6-bottom panel-c). Among our BLL with known redshift, only two are at $z > 0.5$ and the Mg II emission could occur in the observed spectral range. For these sources we estimate an upper limit of the Mg II luminosity $\leq 2 \times 10^{42} \text{ erg/s}$, that is a factor 20 smaller than the average value of the QSOs reported in Shen, et al. (2011). A similar value is also found for the BLL for which we provide a spectroscopic redshift lower limit. As for the case of [O III] lines, when accounting for the same beaming correction data points and limits locate in the region of the lowest luminosity (see Fig. 6-bottom panel-d).

The comparison and contrast of the properties of the emission lines of BLL and AGN obviously requires a thorough and extended discussion, which deserve the comparison of large and homogeneous samples to properly investigate this issue.

DATA AVAILABILITY

The flux calibrated and dereddened spectra are available in our online database ZBLAC⁴.

⁴ <http://web.oapd.inaf.it/zblac/>

Table 1. THE SAMPLE OF THE 3FHL TEV CANDIDATES OBJECTS AND JOURNAL OF THE GTC OBSERVATIONS

3FGL Name	Counterpart	RA (J2000)	DEC (J2000)	Class	E(B-V)	Obs. date	t_{EXP} (s)	Seeing (")	g
3FHLJ0009.4+5030	NVSSJ000922+503028	00:09:22.8	50:30:28.8	bll	0.13	06-11-2018	4500	1.5	18.9
3FHLJ0015.7+5551	GB6J0015+5551	00:15:40.1	55:51:45.0	bll	0.37	06-11-2018	3000	1.5	18.7
3FHLJ0045.3+2127	GB6J0045+2127	00:45:19.3	21:27:40.0	bll	0.03	06-11-2018	1200	1.7	17.7
3FHLJ0045.7+1217	GB6J0045+1217	00:45:43.3	12:17:12.0	bll	0.07	26-11-2018	3000	2.0	17.6
3FHLJ0131.1+6120	1RXSJ013106.4+612035	01:31:07.3	61:20:34.0	bll	0.79	03-12-2018	3600	1.3	20.3
3FHLJ0134.4+2638	1RXSJ013427.2+263846	01:34:28.1	26:38:43.0	bcu	0.09	03-12-2017	1000	1.3	17.6
3FHLJ0137.9+5815	1RXSJ013748.0+581422	01:37:50.4	58:14:11.0	bll	0.45	03-01-2019	3600	1.2	18.9
3FGLJ0141.4-0929	PKS0139-09	01:41:25.8	-09:28:43.7	bll	0.02	27-12-2017	1350	1.1	16.8
3FHLJ0148.2+5201	GB6J0148+5202	01:48:20.2	52:02:06.0	bll	0.19	04-12-2018	2400	2.7	18.1
3FHLJ0241.3+6543	TXS0237+655	02:41:21.6	65:43:11.9	bcu	1.09	07-12-2016	3600	0.9	20.9
3FHLJ0250.5+1712	NVSSJ025037+171209	02:50:37.9	17:12:09.0	bll	0.12	30-10-2018	1200	1.7	17.8
3FHLJ0322.0+2336	MG3J032201+2336	03:22:00.0	23:36:11.0	bll	0.17	30-10-2018	1200	1.3	17.5
3FHLJ0423.8+4149	4C+41.11	04:23:56.0	41:50:02.7	bll	0.63	26-03-2018	7200	1.9	20.3
3FHLJ0433.1+3227	NVSSJ043307+322840	04:33:07.7	32:28:40.0	bll	0.38	08-11-2018	3900	0.7	19.7
3FHLJ0433.6+2905	MG2J043337+2905	04:33:37.8	29:05:55.4	bll	0.66	21-02-2017	4500	1.9	21.9
3FHLJ0434.7+0921	TXS0431+092	04:34:41.0	09:23:49.0	bcu	0.22	05-12-2017	3900	1.6	18.1
3FHLJ0500.3+5238	GB6J0500+5238	05:00:21.4	52:38:02.0	bcu	0.75	26-11-2016	3600	1.4	19.6
3FHLJ0506.0+6113	NVSSJ050558+611336	05:05:58.8	61:13:36.0	bll	0.55	14-12-2018	4800	2.0	19.6
3FHLJ0515.8+1528	GB6J0515+1527	05:15:47.3	15:27:17.0	bll	0.47	03-03-2019	7200	1.7	18.9
3FHLJ0540.5+5823	GB6J0540+5823	05:40:30.0	58:23:38.0	bll	0.34	28-01-2018	900	1.7	18.2
3FHLJ0600.3+1245	NVSSJ060015+124344	06:00:15.0	12:43:43.0	bcu	0.41	28-11-2016	3600	0.9	18.5
3FHLJ0601.0+3837	B20557+38	06:01:02.8	38:38:29.0	bll	0.46	09/10-03-2019	6000	1.6	20.5
3FHLJ0602.0+5316	GB6J0601+5315	06:02:00.4	53:16:00.0	bcu	0.15	03-12-2017	900	1.2	17.0
3FHLJ0607.4+4739	TXS0603+476	06:07:23.2	47:39:47.0	bll	0.16	20-01-2019	1200	1.1	17.2
3FHLJ0612.8+4122	B30609+413	06:12:51.2	41:22:37.0	bll	0.17	20-01-2019	900	1.2	18.1
3FHLJ0620.6+2645	RXJ0620.6+2644	06:20:40.0	26:43:32.0	bcu	0.34	09-04-2019	3600	1.8	18.5
3FHLJ0640.0-1254	TXS0637-128	06:40:07.2	12:53:14.2	bcu	0.49	24-02-2017	1500	1.5	17.9
3FHLJ0702.6-1950	TXS0700-197	07:02:42.9	-19:51:22.0	bll	0.42	10-03-2019	750	1.9	19.1
3FHLJ0706.5+3744	GB6J0706+3744	07:06:31.7	37:44:36.0	bll	0.06	02-11-2018	1800	2.5	17.6
3FHLJ0708.9+2240	GB6J0708+2241	07:08:58.3	22:41:36.0	bll	0.05	03-12-2018	4500	1.2	17.4
3FHLJ0709.1-1525	PKS0706-15	07:09:12.3	-15:27:00.0	bcu	0.55	04-12-2018	7200	2.5	18.9
3FHLJ0723.0-0732	1RXSJ072259.5-073131	07:22:59.7	-07:31:35.0	bll	0.21	14-12-2018	3000	1.2	18.1
3FHLJ0811.9+0237	PMNJ0811+0237	08:12:01.8	02:37:33.0	bll	0.02	04-12-2018	7200	2.0	18.0
3FHLJ0816.4-1311	PMNJ0816-1311	08:16:27.2	-13:11:52.0	bll	0.07	22-02-2018*	5400	1.8	17.2
3FHLJ0905.5+1357	MG1J090534+1358	09:05:35.0	13:58:06.0	bll	0.03	17-02-2018**	850	1.2-2.0	16.2-17.3**
3FHLJ0910.5+3329	Ton1015	09:10:37.0	33:29:24.0	bll	0.02	22-02-2018	350	1.5	16.2
3FHLJ0953.0-0840	PMNJ0953-0840	09:53:02.7	-08:40:18.0	bll	0.04	22-02-2018	900	1.5	16.8
3FHLJ1037.6+5711	GB6J1037+5711	10:37:44.3	57:11:56.0	bll	0.01	30-04-2018	1050	1.2	16.5
3FHLJ1055.6-0125	NVSSJ105534-012617	10:55:34.3	-01:26:16.0	bll	0.04	14-12-2018	3000	1.3	18.6
3FHLJ1059.1-1134	PKSB1056-113	10:59:12.4	-11:34:23.0	bll	0.02	22-01-2019	900	1.8	17.6
3FHLJ1150.5+4154	RBS1040	11:50:34.7	41:54:40.9	bll	0.02	20-01-2019	900	1.3	17.0
3FHLJ1233.7-0145	NVSSJ123341-014426	12:33:41.3	-01:44:24.0	bll	0.03	20-01-2019	3600	1.9	20.3
3FHLJ1253.1+5300	S41250+53	12:53:11.9	53:01:12.0	bll	0.01	20-01-2019	1200	1.2	16.6
3FHLJ1418.4-0233	NVSSJ141826-023336	14:18:26.3	-02:33:34.0	bll	0.05	30-04-2018	1050	1.2	16.4
3FHLJ1445.0-0326	RBS1424	14:45:06.3	-03:26:12.0	bll	0.08	09-04-2019	3600	1.2	17.8
3FHLJ1447.9+3608	RBS1432	14:48:00.6	36:08:32.0	bll	0.01	16-04-2019	1500	1.8	16.2
3FHLJ1454.5+5124	TXS1452+516	14:54:27.1	51:24:34.0	bll	0.02	10-04-2019	3600	1.0	16.7
3FHLJ1503.7-1541	RBS1457	15:03:40.6	-15:41:14.0	bll	0.10	16-04-2019	3600	2.0	17.8
3FHLJ1549.9-0659	NVSSJ154952-065907	15:49:52.0	-06:59:07.0	bcu	0.14	09-04-2018	7200	1.7	18.1
3FHLJ1748.6+7006	S41749+70	17:48:32.8	70:05:50.7	bll	0.03	29-03-2018	1500	0.9	16.6
3FHLJ1800.5+7827	S51803+784	18:00:45.7	78:28:04.0	bll	0.04	11-08-2018	900	2.5	16.7
3FHLJ1841.3+2909	MG3J184126+2910	18:41:21.7	29:09:41.0	bcu	0.21	31-03-2018	1200	1.8	18.2
3FHLJ1904.1+3627	MG2J190411+3627	19:04:11.9	36:26:59.0	bcu	0.08	07-04-2018	1600	2.0	17.3
3FHLJ1911.5-1908	PMNJ1911-1908	19:11:29.7	-19:08:23.0	bcu	0.14	12-05-2018	1200	2.0	18.0
3FHLJ1921.8-1607	PMNJ1921-1607	19:21:51.5	-16:07:13.2	bll	0.16	18-10-2018***	5400	2.5	17.6

Col.1: Fermi name of the target; Col.2: Counterpart name of the target; Col.3 - 4: Right ascension and declination of the optical counterpart; Col.5: Source classification reported in the 3FHL catalog (bll = BL Lac object, bcu = blazar candidate of uncertain type); Col.6: $E(B-V)$ taken from the NASA/IPAC Infrared Science Archive (<https://irsa.ipac.caltech.edu/applications/DUST/>); Col.7: Date of observation; Col.8: Total integration time; Col.9: Seeing during the observation; Col.10: g magnitude measured from the acquisition image.

(*) This source was observed also in 14-12-2018 and 04-04-2019, (**) This source was observed also in 09-03-2019 and the source was found in two different flux states, (***) This source was also discussed in [Paiano et al. \(2017c\)](#)

Table 2. PROPERTIES OF THE OPTICAL SPECTRA OF THE 3FHL SAMPLE

OBJECT	SNR	EW _{min}	z	Line type
3FHLJ0009.4+5030	160	0.17 - 0.20	(> 0.60)	L
3FHLJ0015.7+5551	120	0.25 - 0.40	0.2168	E,G
3FHLJ0045.3+2127	90	0.30	0.4253	G
3FHLJ0045.7+1217	200	0.20	0.2549	G
3FHLJ0131.1+6120	75	0.20 - 0.70	(> 0.10)	L
3FHLJ0134.4+2638	80	0.35 - 0.50	(> 0.15)	L
3FHLJ0137.9+5815	145	0.25 - 0.30	0.2745	G
3FGLJ0141.4-0929	200	0.20	≥ 0.501	I
3FHLJ0148.2+5201	110	0.30 - 0.35	0.437	G
3FHLJ0241.3+6543	25	1.10 - 2.70	0.1211	E,G
3FHLJ0250.5+1712	100	0.35 - 0.45	0.2435	G
3FHLJ0322.0+2336	160	0.10 - 0.25	(> 0.25)	L
3FHLJ0423.8+4149	40	0.35 - 1.60	0.3977	E
3FHLJ0433.1+3227	110	0.25 - 0.35	(> 0.45)	L
3FHLJ0433.6+2905	15	1.35 - 3.80	0.91 ?	E
3FHLJ0434.7+0921	75	0.30 - 0.90	(> 0.1)	L
3FHLJ0500.3+5238	40	0.55 - 4.00	0.1229	E,G
3FHLJ0506.0+6113	70	0.30 - 0.90	0.538 ?	G
3FHLJ0515.8+1528	130	0.20 - 0.30	(> 0.20)	L
3FHLJ0540.5+5823	60	0.40 - 0.90	(> 0.10)	L
3FHLJ0600.3+1245	50	0.45 - 1.85	0.0835	E,G
3FHLJ0601.0+3837	40	0.50 - 1.35	0.662 ?	G
3FHLJ0602.0+5316	70	0.35 - 1.00	0.0522	G
3FHLJ0607.4+4739	100	0.15 - 0.40	(> 0.10)	L
3FHLJ0612.8+4122	50	0.35 - 1.10	≥1.107	I
3FHLJ0620.6+2645	75	0.40 - 0.80	0.1329	G
3FHLJ0640.0-1254	80	0.35 - 0.65	0.1365	E,G
3FHLJ0702.6-1950	50	0.50 - 0.95	(> 0.10)	L
3FHLJ0706.5+3744	100	0.20 - 0.35	≥0.1042	I
3FHLJ0708.9+2240	250	0.15 - 0.20	0.2966	G
3FHLJ0709.1-1525	70	0.35 - 1.10	0.1420	E,G
3FHLJ0723.0-0732	170	0.10 - 0.25	0.3285	G
3FHLJ0811.9+0237	70	0.40 - 0.85	0.1726	E,G
3FHLJ0816.4-1311	300	0.10	(> 0.40)	L
3FHLJ0905.5+1357	200	0.10 - 0.20	0.2239:	E
3FHLJ0910.5+3329	200	0.10 - 0.20	(> 0.15)	L
3FHLJ0953.0-0840	220	0.15 - 0.25	(> 0.15)	L
3FHLJ1037.6+5711	300	0.10 - 0.15	(> 0.25)	L
3FHLJ1055.6-0125	130	0.20 - 0.40	(> 0.55)	L
3FHLJ1059.1-1134	50	0.30 - 1.15	(> 0.10)	L
3FHLJ1150.5+4154	200	0.15 - 0.25	(> 0.25)	L
3FHLJ1233.7-0145	40	0.45 - 0.95	(> 0.10)	L
3FHLJ1253.1+5300	250	0.10 - 0.20	≥0.6638	I
3FHLJ1418.4-0233	200	0.15 - 0.30	(> 0.12)	L
3FHLJ1445.0-0326	200	0.10 - 0.20	(> 0.45)	L
3FHLJ1447.9+3608	250	0.10 - 0.20	≥0.738	I
3FHLJ1454.5+5124	320	0.05 - 0.10	(> 0.40)	L
3FHLJ1503.7-1541	50	0.55 - 1.25	(> 0.10)	L
3FHLJ1549.9-0659	200	0.15 - 0.20	0.418	G
3FHLJ1748.6+7006	320	0.10 - 0.20	(> 0.3)	L
3FHLJ1800.5+7827	130	0.25 - 0.40	0.683	E
3FHLJ1841.3+2909	40	0.55 - 1.35	(> 0.10)	L
3FHLJ1904.1+3627	60	0.40 - 1.50	0.08977	G
3FHLJ1911.5-1908	50	0.55 - 1.20	0.138	E,G
3FHLJ1921.8-1607	125	0.20 - 0.50	(> 0.12)	L

Col.1: Name of the target; Col.2: Median S/N of the spectrum; Col.3: Range of the minimum equivalent width (EW_{min}) derived from different regions of the spectrum; Col.4: Redshift; Col.5: Type of detected line to estimate the redshift: *E* = emission line, *G* = galaxy absorption line, *I* = intervening absorption assuming Mg II 2800Å identification, *L* = lower limit derived on the lack of detection of host galaxy absorption lines assuming a BLL elliptical host galaxy with M(R) = -22.9 (see details in [Paiano et al. 2017a](#)).

(:) This marker indicates that the redshift is tentative due to the detection of only one feature.

(*) For this source we found other two absorption line systems due to Fe II (2382, 2600) (See details text).

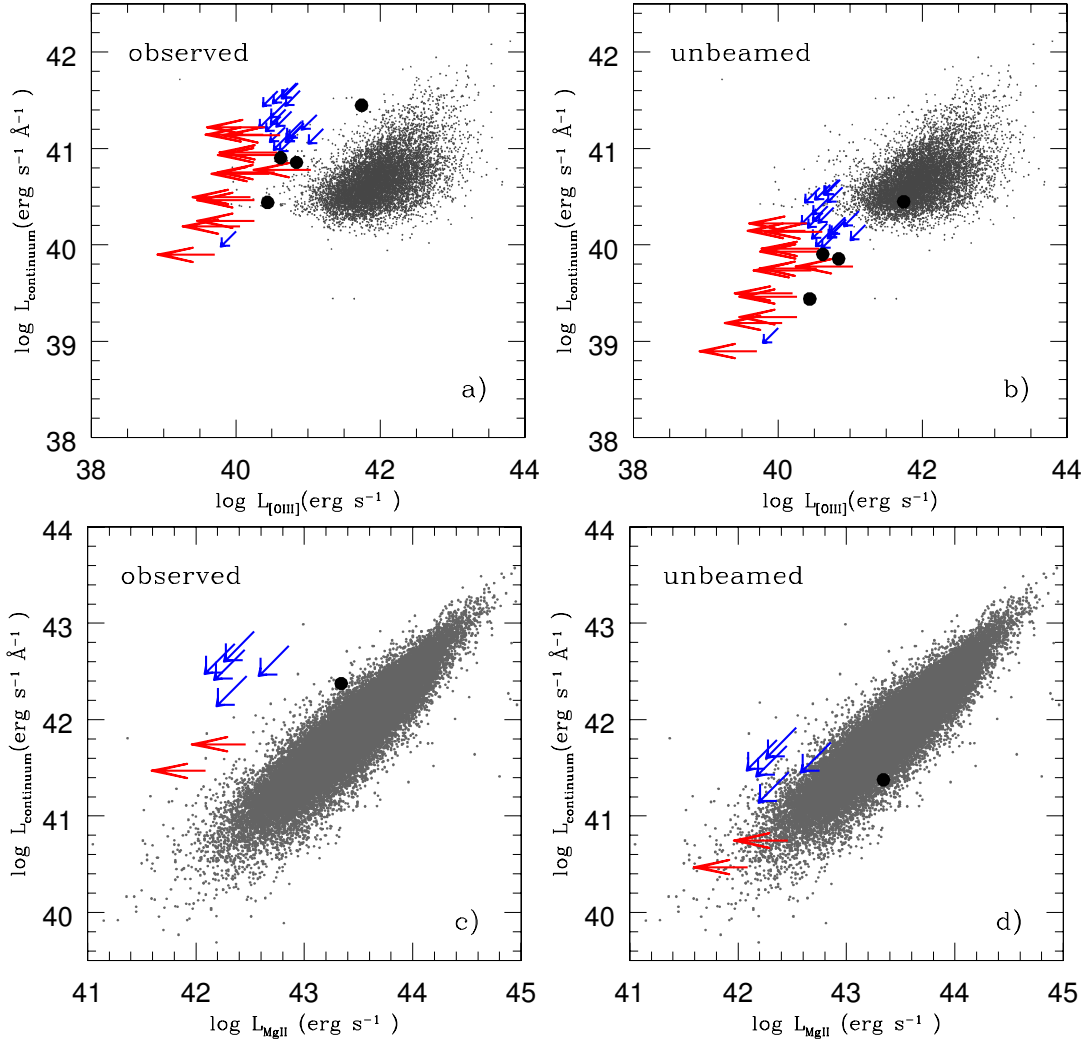


Figure 6. *Upper panels:* The relation between the [O III] line luminosity and the beamed (on the left) and unbeamed of a factor ten (on the right) continuum luminosity of our sample of 3FHL BLL compared to that of low redshift ($0.1 < z < 0.5$) QSOs from SDSS (grey points) taken from Shen, et al. (2011). The four cases with detected [O III] emission line are marked with black circles (see also Table 3). The 13 BLL with known redshift but without the [O III] line detection are indicated as red arrows and represent upper limits for $L_{[\text{OIII}]}$. Finally the blue arrows are the upper limits for [O III] and continuum luminosity for the BLL without redshift (see text for details). *Bottom panels:* The relation between the Mg II line luminosity and the beamed (on the left) and unbeamed of a factor ten (on the right) continuum luminosity of our BLL sample compared to that of QSO ($0.46 < z < 1.5$) from Shen, et al. (2011). The only case with Mg II line detected is marked with black circle, the two sources with $z > 0.5$ and without Mg II line detection are marked as red arrows, while the BLL with spectroscopic redshift lower limit are labelled with blue arrows.

REFERENCES

- Abdollahi S., et al., 2020, ApJS, 247, 33
 Ahlers M., Halzen F., 2015, RPPPh, 78, 126901
 Ajello M., et al., 2017, ApJS, 232, 18
 Ajello M., et al., 2014, ApJ, 780, 73
 Álvarez Crespo N., et al., 2016, AJ, 151, 32
 Archambault S., et al., 2016, AJ, 151, 142
 Bauer F. E., Condon J. J., Thuan T. X., Broderick J. J., 2000, ApJS, 129, 547
 Bressan A., Falomo R., Valdés J. R., Rampazzo R., 2006, ApJL, 645, L101
 Caccianiga A., Marchã M. J., Antón S., Mack K.-H., Neeser M. J., 2002, MNRAS, 329, 877
 Cardelli J. A., Clayton G. C., Mathis J. S., 1989, ApJ, 345, 245
 Cepa J., et al., 2003, SPIE, 4841, 1739, SPIE.4841
 Cusumano G., et al., 2010, A&A, 524, A64
 D’Abrusco R., Massaro F., Paggi A., Smith H. A., Masetti N., Landoni M., Tosti G., 2014, ApJS, 215, 14
 D’Abrusco R., et al., 2019, ApJS, 242, 4
 Falomo R., Scarpa R., Treves A., Urry C. M., 2000, ApJ, 542, 731
 Falomo R., Pian E., Treves A., 2014, A&ARv, 22, 73
 Falomo R., Treves A., Scarpa R., Paiano S., Landoni M., 2017, MNRAS, 470, 2814
 Fermi-LAT collaboration, 2019, arXiv, arXiv:1905.10771
 Franceschini A., Rodighiero G., 2017, A&A, 603, A34
 Ghisellini G., Tavecchio F., 2009, MNRAS, 397, 985
 Ghisellini G., Righi C., Costamante L., Tavecchio F., 2017, MNRAS, 469, 255
 Giommi P., Perri M., Piranomonte S., Padovani P., 2002, babs.conf, 123, babs.conf
 Giommi P., Padovani P., Polenta G., 2013, MNRAS, 431, 1914
 Hewitt A., Burbidge G., 1993, ApJS, 87, 451
 Kügler S. D., Nilsson K., Heidt J., Esser J., Schultz T., 2014,

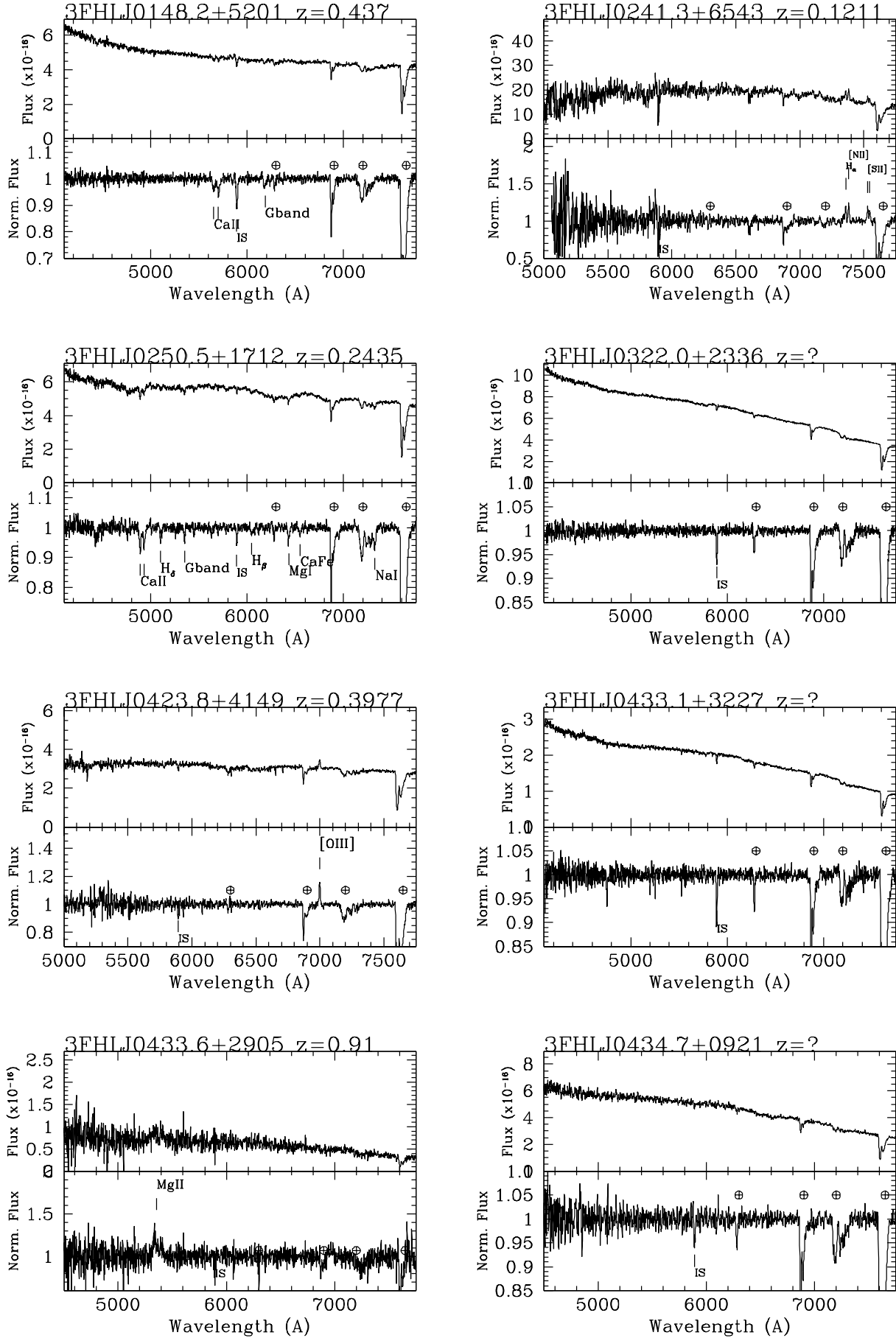


Figure 1. - Continued -

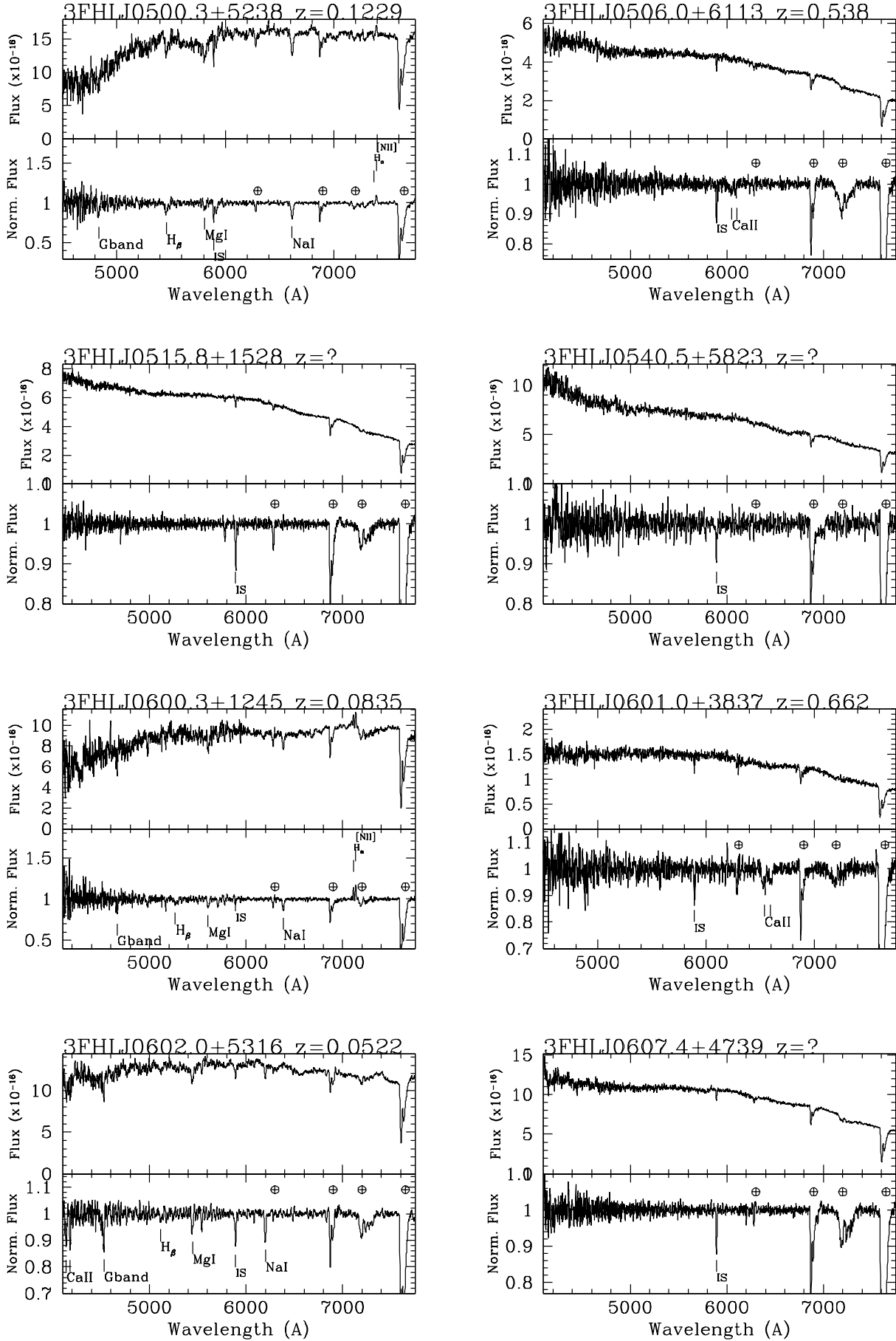


Figure 1. - Continued -

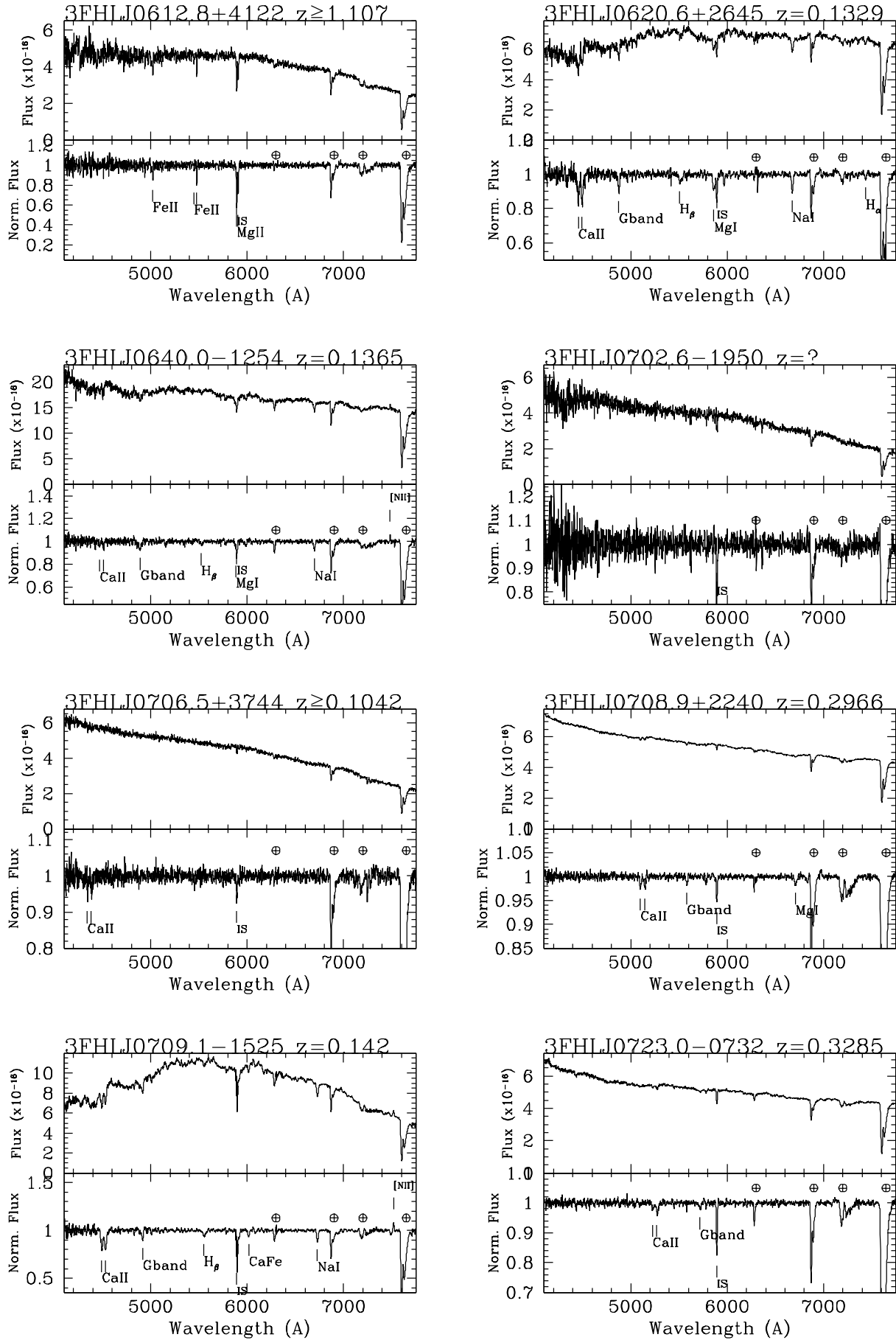


Figure 1. - Continued -

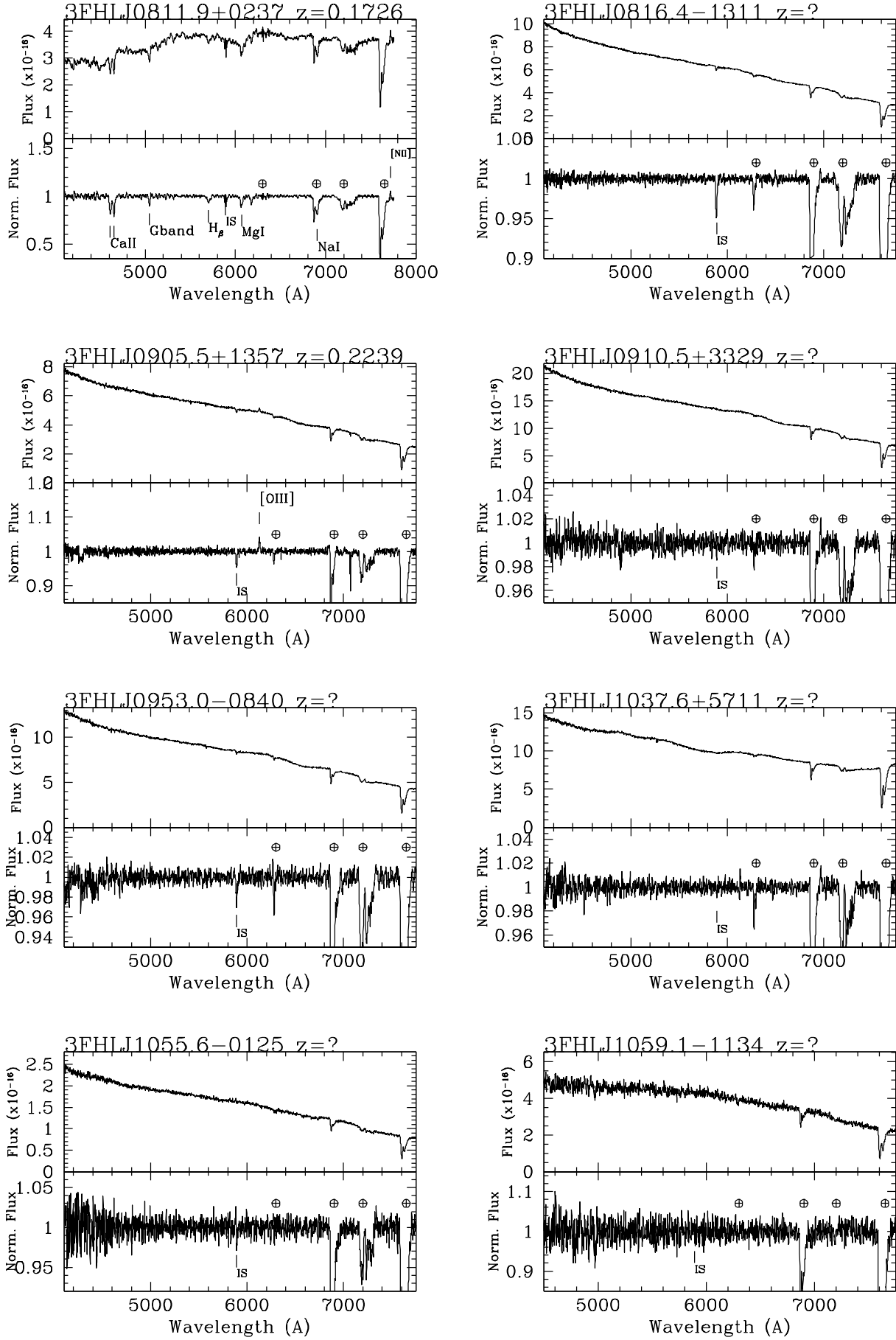


Figure 1. - Continued -

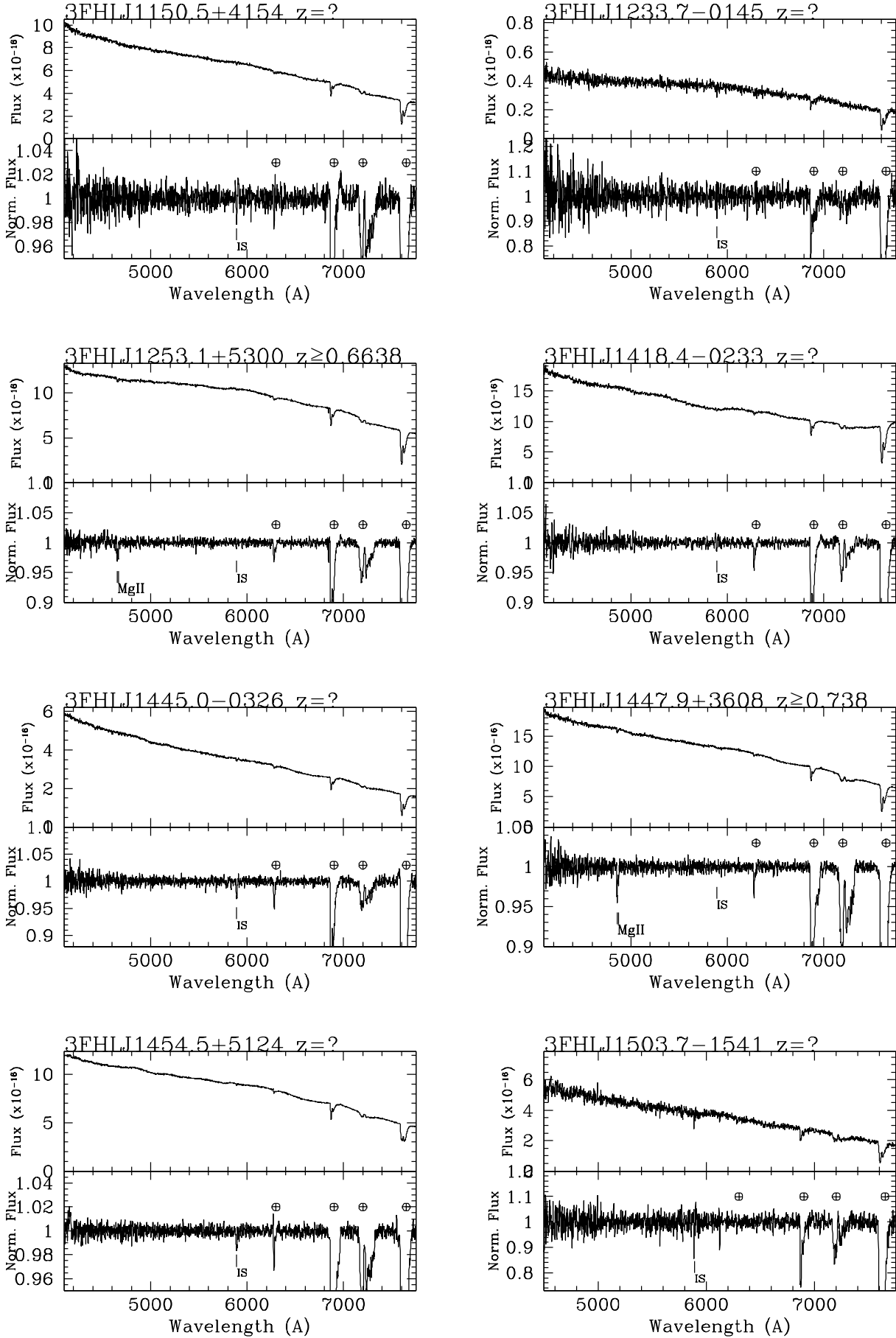


Figure 1. - Continued -

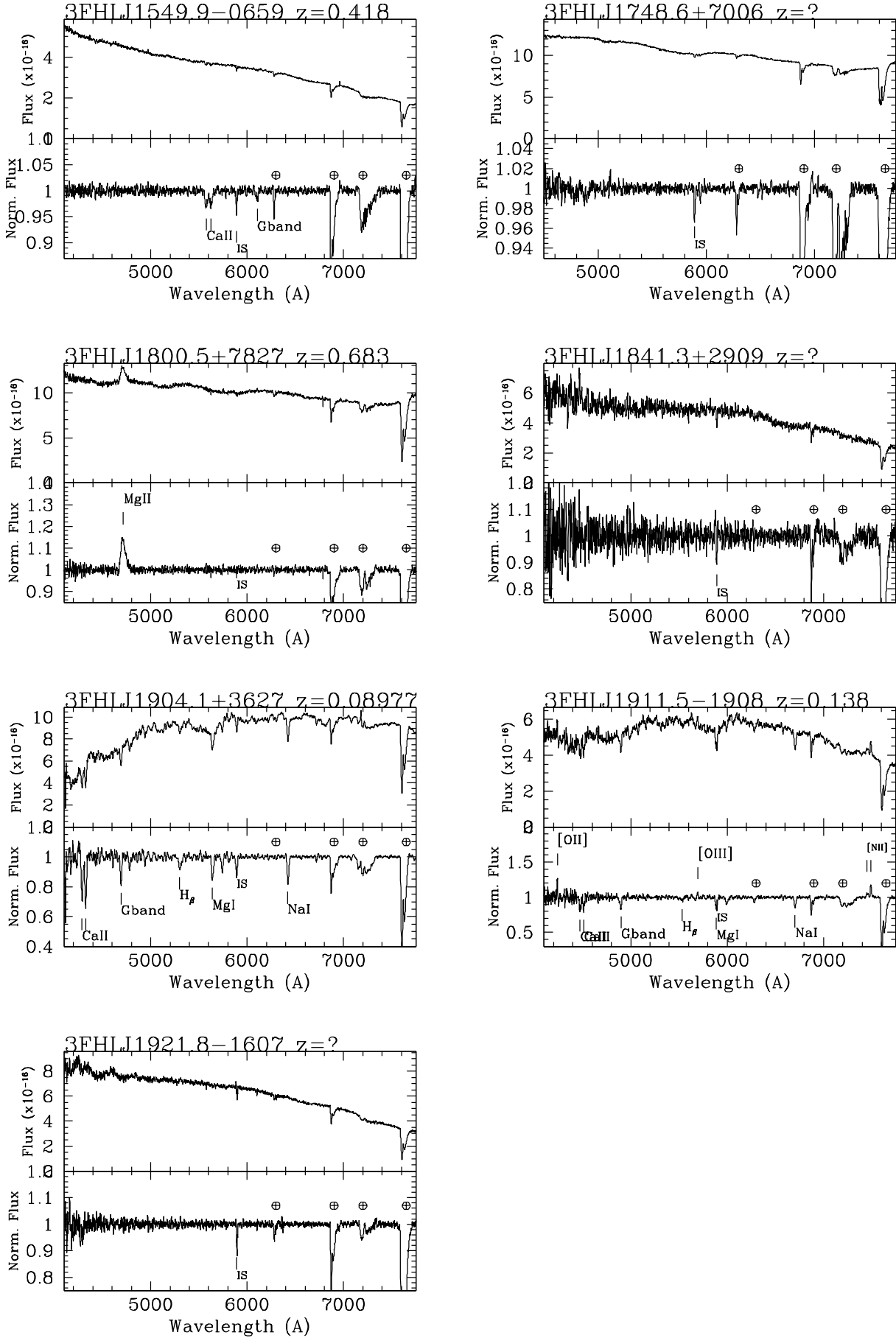


Figure 1. - Continued -

Table 3. MEASUREMENTS OF THE DETECTED LINES

Object name	λ (Å)	EW (Å)	Line ID	Line Lum. (erg/s)
3FHLJ0015.7+5551	4787	1.6	Ca II 3934	4.2×10^{40}
	4829	1.0	Ca II 3968	
	5238	1.0	G-band 4305	
	6093	-0.5	[O III] 5007	
	6411	0.4	Ca+Fe 5269	
3FHLJ0045.3+2127	5607	1.0	Ca II 3934	2.3×10^{40}
	5656	0.5	Ca II 3968	
3FHLJ0045.7+1217	4679	-0.2	[O II] 3727	
	4936	1.0	Ca II 3934	
	4980	0.9	Ca II 3968	
	5403	0.3	G-band 4305	
	6489	0.6	Mg I 5175	
	6612	0.5	Ca+Fe 5269	
	7393	0.5	Na I 5892	
3FHLJ0137.9+5815	5013	0.4	Ca II 3934	1.3×10^{41}
	5057	0.6	Ca II 3968	
	6596	0.9	Mg I 5175	
3FGLJ0141.4-0929	4197	1.0	Mg II 2796	2.0×10^{41}
	4207	0.5	Mg II 2803	
3FHLJ0148.2+5201	5654	1.3	Ca II 3934	1.3×10^{41}
	5703	1.5	Ca II 3968	
	6183	0.8	G-band 4305	
3FHLJ0241.3+6543	6607	2.8	Na I 5892	8.7×10^{40}
	7358	-1.7	H α 6563	
	7381	-2.5	[N II] 6584	
	7531	-2.0	[SII] 6716	
	7545	-1.4	[SII] 6731	
3FHLJ0250.5+1712	4890	1.7	Ca II 3934	5.5×10^{41}
	4932	1.5	Ca II 3968	
	5090	0.5	H δ 4102	
	5352	0.6	G-band 4305	
	6045	0.6	H β 4861	
	6433	0.8	Mg I 5175	
	6549	0.6	Ca+Fe 5269	
3FHLJ0423.8+4149	7324	1.9	Na I 5892	2.5×10^{42}
	6998	-1.9	[O III] 5007	
3FHLJ0433.6+2905	~5340	-9.5	Mg II 2800	1.7×10^{40}
3FHLJ0500.3+5238	4833	3.5	G-band 4305	
	5459	3.1	H β 4861	8.7×10^{40}
	5811	1.6	Mg I 5175	
	5917	2.3	Ca+Fe 5269	2.3×10^{40}
	6617	4.7	Na I 5892	
3FHLJ0506.0+6113	7369	-0.3	H α 6563	3.5×10^{40}
	7393	-1.3	[N II] 6584	
3FHLJ0600.3+1245	6042	0.8	Ca II 3934	2.3×10^{40}
	6096	0.6	Ca II 3968	
3FHLJ0601.0+3837	4664	1.6	G-band 4305	2.3×10^{40}
	5267	1.8	H β 4861	
	5608	2.3	Mg I 5175	
	5709	1.6	Ca+Fe 5269	
	6385	3.1	Na I 5892	
	7111	-1.2	H α 6563	
	7133	-1.8	[N II] 6584	
3FHLJ0601.0+3837	6538	2.5	Ca II 3934	3.5×10^{40}
	6596	2.0	Ca II 3968	

Col. 1: Name of the target; Col. 2: Barycenter of the detected line; Col. 3: Measured equivalent width; Col. 4: Line identification; Col. 5: Line luminosity.

Table 3. MEASUREMENTS OF THE DETECTED LINES

Object name	λ (Å)	EW (Å)	Line ID	Line Lum. (erg/s)
3FHLJ0602.0+5316	4139	2.8	Ca II 3934	4.7×10^{40}
	4176	1.5	Ca II 3968	
	4529	2.1	G-band 4305	
	5115	0.6	H β 4861	
	5446	1.3	Mg I 5175	
3FHLJ0612.8+4122	5543	0.7	Ca+Fe 5269	4.7×10^{40}
	6200	1.8	Na I 5892	
3FHLJ0620.6+2645	5022	1.5	Fe II 2382	4.7×10^{40}
	5450	0.4	Fe II 2586	
	5478	1.5	Fe II 2600	
	5891	3.5	Mg II 2796	
	5906	3.1	Mg II 2803	
	4456	2.8	Ca II 3934	
	4496	3.7	Ca II 3968	
3FHLJ0640.0-1254	4876	1.7	G-band 4305	4.7×10^{40}
	5507	1.2	H β 4861	
	5863	2.6	Mg I 5175	
	5969	0.8	Ca+Fe 5269	
	6676	2.1	Na I 5892	
	7435	0.4	H α 6563	
	4471	0.4	Ca II 3934	
3FHLJ0706.5+3744	4510	0.8	Ca II 3968	4.7×10^{40}
	4892	1.6	G-band 4305	
	5525	0.7	H β 4861	
	5882	2.2*	Mg I 5175	
	5988	0.7	Ca+Fe 5269	
	6697	1.4	Na I 5892	
	7482	-0.6	[N II] 6584	
3FHLJ0708.9+2240	4344	0.4	Ca II 3934	3.4×10^{40}
	4382	0.6	Ca II 3968	
3FHLJ0709.1-1525	5100	0.4	Ca II 3934	3.4×10^{40}
	5146	0.5	Ca II 3968	
	5581	0.3	G-band 4305	
	6710	0.5	Mg I 5175	
	6832	0.2	Ca+Fe 5269	
	4492	5.3	Ca II 3934	
	4532	4.6	Ca II 3968	
3FHLJ0723.0-0732	4916	1.7	G-band 4305	3.4×10^{40}
	5552	1.9	H β 4861	
	6017	1.3	Ca+Fe 5269	
	6729	2.3	Na I 5892	
	7518	-1.0	[N II] 6584	
	5226	0.5	Ca II 3934	
	5272	0.9	Ca II 3968	
3FHLJ0811.9+0237	5718	0.5	G-band 4305	9.8×10^{39}
	4613	4.7	Ca II 3934	
	4653	4.5	Ca II 3968	
	5047	1.6	G-band 4305	
	5700	2.7	H β 4861	
	6069	3.0	Mg I 5175	
	6178	1.9	Ca+Fe 5269	
3FHLJ0905.5+1357	6910	6.0*	Na I 5892	$8 \times 10^{40**}$
	7720	-0.3	[N II] 6584	
3FHLJ1253.1+5300	6128	-0.7**	[O III] 5007	$8 \times 10^{40**}$
	4652	0.3	Mg II 2796	
	4664	0.2	Mg II 2803	

(*) This marker indicates that the line is partially contaminated by a telluric band or the interstellar Na I absorption of our Galaxy,

(**) This is the average EW (EW = 0.5 Å when the source is in high state and EW = 0.9 Å in the low state).

Table 3. MEASUREMENTS OF THE DETECTED LINES

Object name	λ (Å)	EW (Å)	Line ID	Line Lum. (erg/s)
3FHLJ1447.9+3608	4859	0.4	Mg II 2796	
	4872	0.2	Mg II 2803	
3FHLJ1549.9-0659	5578	1.1	Ca II 3934	
	5627	0.9	Ca II 3968	
	6104	0.5	G-band 4305	
3FHLJ1800.5+7827	4712	-8.3	Mg II 2800	2.2×10 ⁴³
3FHLJ1904.1+3627	4287	6.0	Ca II 3934	
3FHLJ1911.5-1908	4325	5.9	Ca II 3968	8.3×10 ⁴⁰
	4691	3.6	G-band 4305	
	5298	2.6	H β 4861	
	5640	3.5	Mg I 5175	
	5742	2.1	Ca+Fe 5269	
	6421	3.6	Na I 5892	
	4242	-2.8	[O II] 3727	
	4474	4.1	Ca II 3934	
	4514	2.9	Ca II 3968	
	4896	3.3	G-band 4305	
	5529	1.3	H β 4861	
	5695	-0.9	[O III] 5007	
	5886	3.3	Mg I 5175	
	5993	2.2	Ca+Fe 5269	
	6702	3.0	Na I 5892	
	7448	-0.7*	[N II] 6548	1.5×10 ⁴⁰
	7465	-0.6*	H α 6563	1.3×10 ⁴³
	7489	-2.6	[N II] 6584	6.3×10 ⁴⁰

(*) These lines are very faint and blended.

- A&A, 569, A95
- Landi R., Bassani L., Stephen J. B., Masetti N., Malizia A., Ubertini P., 2015, A&A, 581, A57
- Landoni M., Falomo R., Treves A., Sbarufatti B., Decarli R., Tavecchio F., Kotilainen J., 2012, A&A, 543, A116
- Landoni M., Falomo R., Treves A., Sbarufatti B., Barattini M., Decarli R., Kotilainen J., 2013, AJ, 145, 114
- Landoni M., Falomo R., Treves A., Sbarufatti B., 2014, A&A, 570, A126
- Landoni M., Falomo R., Treves A., Scarpa R., Reverte Payá D., 2015, AJ, 150, 181
- Landoni M., Paiano S., Falomo R., Scarpa R., Treves A., 2018, ApJ, 861, 130
- Laurent-Muehleisen S. A., Kollgaard R. I., Ciardullo R., Feigelson E. D., Brinkmann W., Siebert J., 1998, ApJS, 118, 127
- Laurent-Muehleisen S. A., Kollgaard R. I., Feigelson E. D., Brinkmann W., Siebert J., 1999, ApJ, 525, 127
- Lawrence C. R., Zucker J. R., Readhead A. C. S., Unwin S. C., Pearson T. J., Xu W., 1996, ApJS, 107, 541
- Madejski G., Sikora M., 2016, ARA&A, 54, 725
- Maraschi L., Ghisellini G., Celotti A., 1992, ApJL, 397, L5
- Marchã M. J. M., Caccianiga A., 2013, MNRAS, 430, 2464
- Marchesi S., Kaur A., Ajello M., 2018, AJ, 156, 212
- Martí J., Paredes J. M., Bloom J. S., Casares J., Ribó M., Falco E. E., 2004, A&A, 413, 309
- Massaro F., Paggi A., Errando M., D'Abrusco R., Masetti N., Tosti G., Funk S., 2013, ApJS, 207, 16
- Massaro F., et al., 2015, A&A, 575, A124
- Meisner A. M., Romani R. W., 2010, ApJ, 712, 14
- Padovani P., Resconi E., Giommi P., Arsioli B., Chang Y. L., 2016, MNRAS, 457, 3582
- Paggi A., et al., 2014, AJ, 147, 112
- Paiano S., Landoni M., Falomo R., Scarpa R., Treves A., 2016, MNRAS, 458, 2836
- Paiano S., Franceschini A., Stamerra A., 2017, MNRAS, 468, 4902
- Paiano S., Landoni M., Falomo R., Treves A., Scarpa R., Righi C., 2017, ApJ, 837, 144
- Paiano S., Landoni M., Falomo R., Treves A., Scarpa R., 2017, ApJ, 844, 120
- Paiano S., Falomo R., Franceschini A., Treves A., Scarpa R., 2017, ApJ, 851, 135
- Paiano S., Falomo R., Treves A., Scarpa R., 2018, ApJL, 854, L32
- Paiano S., Falomo R., Treves A., Landoni M., Scarpa R., 2018, ATel, 12269, 1
- Paiano S., Falomo R., Treves A., Franceschini A., Scarpa R., 2019, ApJ, 871, 162
- Paiano S., Falomo R., Treves A., Righi C., Scarpa R., Lindfors E., 2019, ATel, 12802, 1
- Paiano S., Padovani P., Falomo R., Giommi P., Scarpa R., Treves A., 2019, ATel, 13202, 1
- Perlman E. S., et al., 1996, ApJS, 104, 251
- Perlman E. S., Padovani P., Giommi P., Sambruna R., Jones L. R., Tzioumis A., Reynolds J., 1998, AJ, 115, 1253
- Piranomonte S., Perri M., Giommi P., Landt H., Padovani P., 2007, A&A, 470, 787
- Pita S., et al., 2014, A&A, 565, A12
- Plotkin R. M., et al., 2010, AJ, 139, 390
- Righi C., Tavecchio F., Inoue S., 2019, MNRAS, 483, L127
- Righi C., Tavecchio F., Pacciani L., 2019, MNRAS, 484, 2067
- Sbarufatti B., Treves A., Falomo R., Heidt J., Kotilainen J., Scarpa R., 2005, AJ, 129, 559
- Sbarufatti B., Treves A., Falomo R., 2005, ApJ, 635, 173
- Sbarufatti B., Treves A., Falomo R., Heidt J., Kotilainen J., Scarpa R., 2006, AJ, 132, 1
- Sbarufatti B., Falomo R., Treves A., Kotilainen J., 2006, A&A, 457, 35
- Sbarufatti B., Ciprini S., Kotilainen J., Decarli R., Treves A., Veronesi A., Falomo R., 2008, arXiv, arXiv:0810.3563
- Sbarufatti B., Ciprini S., Kotilainen J., Decarli R., Treves A., Veronesi A., Falomo R., 2009, AJ, 137, 337
- Scarpa R., Urry C. M., Falomo R., Pesce J. E., Treves A., 2000, ApJ, 532, 740
- Scarpa R., Urry C. M., Padovani P., Calzetti D., O'Dowd M., 2000, ApJ, 544, 258
- Schlaflly E. F., Finkbeiner D. P., 2011, ApJ, 737, 103
- Shaw M. S., et al., 2013, ApJ, 764, 135
- Shen Y., et al., 2011, ApJS, 194, 45
- Stephen J. B., Bassani L., Landi R., Malizia A., Sguera V., Bazzano A., Masetti N., 2010, MNRAS, 408, 422
- Stickel M., Fried J. W., Kuehr H., 1989, A&AS, 80, 103
- Stickel M., Padovani P., Urry C. M., Fried J. W., Kuehr H., 1991, ApJ, 374, 431
- Stickel M., Fried J. W., Kuehr H., 1993, A&AS, 98, 393
- Stickel M., Meisenheimer K., Kuehr H., 1994, A&AS, 105, 211
- Stoeckle J. T., Morris S. L., Gioia I., Maccacaro T., Schild R. E., Wolter A., 1990, ApJ, 348, 141
- Stoeckle J. T., Rector T. A., 1997, ApJL, 489, L17
- Takeuchi Y., Kataoka J., Maeda K., Takahashi Y., Nakamori T., Tahara M., 2013, ApJS, 208, 25
- Tody D., 1986, SPIE, 627, 733, SPIE..627
- Tody D., 1993, ASPC, 52, 173, ASPC...52
- Urry C. M., Padovani P., 1995, PASP, 107, 803
- Urry C. M., Scarpa R., O'Dowd M., Falomo R., Pesce J. E., Treves A., 2000, ApJ, 532, 816
- van Dokkum P. G., 2001, PASP, 113, 1420
- Voges W., et al., 1999, A&A, 349, 389
- Zakamska N. L., et al., 2003, AJ, 126, 2125
- Zhu G., Ménard B., 2013, ApJ, 770, 130

This paper has been typeset from a $\text{\TeX}/\text{\LaTeX}$ file prepared by the author.